iScience

CellPress
OPEN ACCESS

Article

Effective wound healing on diabetic mice by adhesive antibacterial GNPs-lysine composited hydrogel

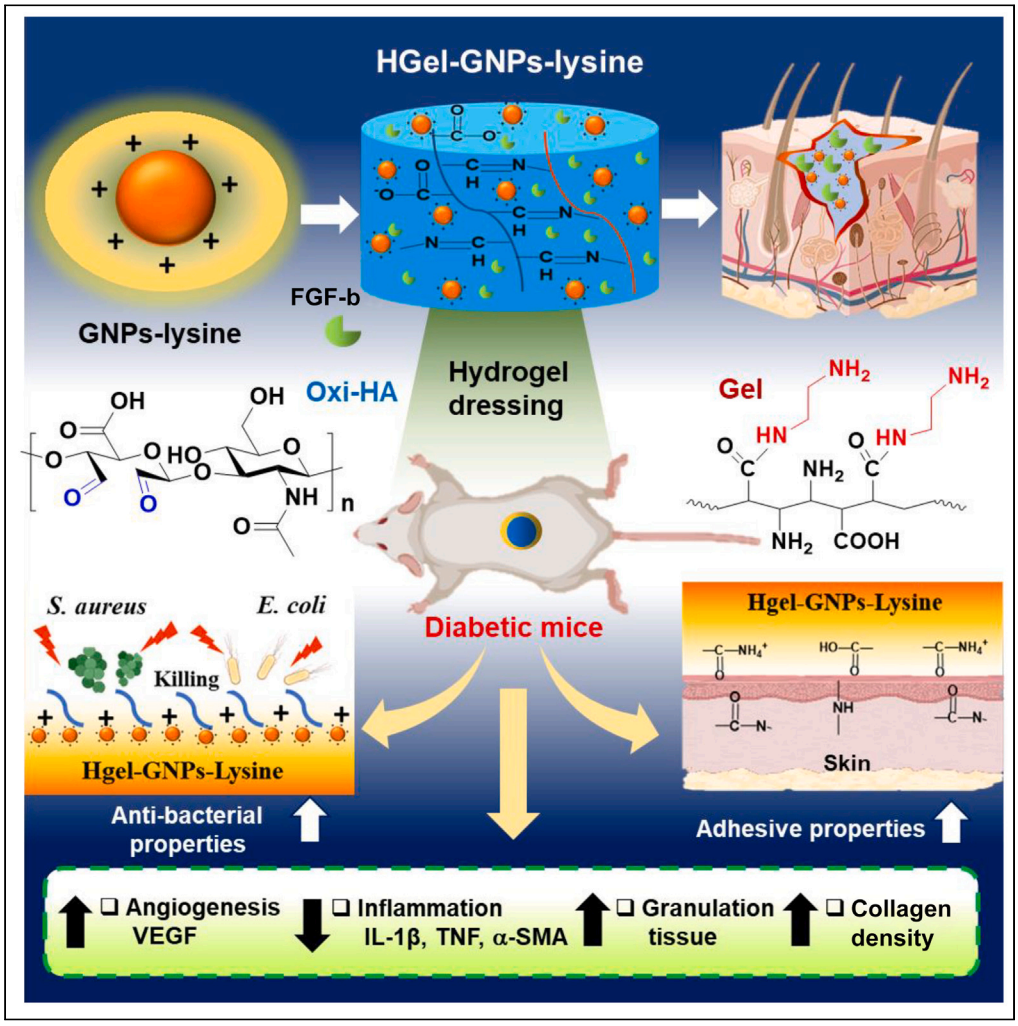

Sureerat Khunmanee, Anseo Choi, Il Young Ahn, Woo Ju Kim, Tae Hui Bae, Shin Hyuk Kang, Hansoo Park

kangshinhyeok@cau.ac.kr (S.H.K.)
heyshoo@cau.ac.kr (H.P.)

Highlights

HGel-GNPs-lysine improved mechanical and tissue adhesive properties

HGel-GNPs-lysine demonstrated antibacterial efficacy against *E. coli* and *S. aureus*

The combination of HGel-GNPs-lysine with FGF-b promoted angiogenesis

HGel-GNPs-lysine+FGF-b reduced inflammation at the wound site in diabetic mice

Khunmanee et al., iScience 27, 108860
February 16, 2024
https://doi.org/10.1016/j.isci.2024.108860

iScience

CellPress
OPEN ACCESS

Article

Effective wound healing on diabetic mice by adhesive antibacterial GNPs-lysine composited hydrogel

Sureerat Khunmanee,[1,4] Anseo Choi,[1,4] Il Young Ahn,[2] Woo Ju Kim,[3] Tae Hui Bae,[3] Shin Hyuk Kang,[2,*] and Hansoo Park[1,5,*]

SUMMARY

Current trends in wound care research focus on creating dressings for diverse wound types, aiming to effectively control the wound healing process. We proposed a wound dressing composed of oxidized hyaluronic acid and amine gelatin with embedded lysine-modified gelatin nanoparticles (HGel-GNPs-lysine). This dressing improves mechanical properties and reduces degradation rates. The storage modulus for HGel-GNPs-lysine was 3,800 Pa, exceeding that of HGel (1,750 Pa). The positively charged surface of GNPs-lysine effectively eliminated *Escherichia coli* and *Staphylococcus aureus*. In a diabetic mice model (C57BL/6), HGel-GNPs-lysine immobilized with basic-fibroblast growth factor promoted granulation tissue thickness and collagen density. Gene expression analysis indicated that HGel-GNPs-lysine reduced inflammation and enhanced angiogenesis. This study highlights that HGel-GNPs-lysine could offer alternative treatment strategies for regulating the inflammatory response at the injury site in wound dressing applications.

INTRODUCTION

Wound healing is a complex process involving multiple tissue cells and stages: hemostasis, inflammation, proliferation, and remodeling. Chronic diabetic wounds are a global concern due to their high morbidity, mortality, and healthcare costs.[1] These wounds differ from acute ones as they have prolonged inflammation and a complex microenvironment. Additionally, diabetic wounds are more likely to become infected, which accelerates tissue damage and inflammation.[2] Bacteria and damaged cells release harmful substances that promote inflammation and inhibit healing.[3] Several treatments have been used to treat chronic wounds, such as hyperbaric oxygen therapy, ultrasound and electromagnetic therapies, skin grafts, and wound dressing.[4]

Hydrogels are three-dimensional (3D) network polymers with versatile properties, including adjustability in terms of chemistry, physics, and biological properties. They offer excellent biocompatibility and responsiveness to pH, light, and temperature changes, making them ideal for various applications, including wound dressing.[5,6] Hydrogels have proven effective in treating diabetic and infected wounds due to their ability to promote tissue adhesion, resist bacteria, encourage cell proliferation, and regulate the local immune system.[7,8] However, their limited thermal stability at high temperatures and mechanical strength have restricted their application. Therefore, it is challenging for the hydrogel dressings that are currently available to achieve the proper equilibrium of physical, chemical, and biological properties.[9]

Numerous methods have been developed to enhance the mechanical strength and degradation of hydrogels. These methods include double crosslink, hydrogen bonding, and nanocomposite hydrogels.[10,11] Nanocomposite hydrogels are a material in which a polymer serves as the matrix, and nanoparticles act as the reinforcing phase to improve stability and strength.[12–14] In other words, nanocomposite hydrogels are created by crosslink hydrophilic polymer networks through covalent chemical bonds or physical crosslinks with nanoparticles, resulting in intricate nanoscale structures.[15–17] However, a well-designed composite may offer unique properties different from the individual component. Fei R. et al. utilized inorganic polysiloxane nanoparticles to form a thermoresponsive poly(N-isopropylacrylamide) double network hydrogels.[18] The compressive and tensile modulus of double network hydrogels was greater than those of single-networks. Mesoporous silica nanoparticles (MSNs) can serve as chemical crosslinkers for polyethylene glycol through dynamic thiol-disulfide covalent interactions. These nanocomposites exhibited rapid self-healing properties, increased storage modulus, and slowly degrade compared with non-composite

[1]Department of Integrative Engineering, Chung-Ang University, 84 Heukseok-ro, Dongjak-gu, Seoul 06974, South Korea
[2]Department of Plastic and Reconstructive Surgery, Chung-Ang University Hospital, Chung-Ang University College of Medicine, 102 Heukseok-ro, Dongjak-gu 06973, South Korea
[3]Department of Plastic and Reconstructive Surgery, Chung-Ang University Gwangmyeong Hospital, Deokan-ro, Gwangmyeong-si, Gyeonggi-do 14353, South Korea
[4]These authors contributed equally
[5]Lead contact
*Correspondence: kangshinhyeok@cau.ac.kr (S.H.K.), heyshoo@cau.ac.kr (H.P.)
https://doi.org/10.1016/j.isci.2024.108860

hydrogel. In wound healing applications, silver, gold, and copper nanoparticles have been used to promote angiogenesis and endothelial cell proliferation while accelerating wound closure, enhancing antibacterial and antioxidant characteristics.[19–24]

Recently, wound dressing systems have prioritized natural polymer hydrogel dressings that can enhance the wound microenvironment and promote healing at different stages.[25–27] Methacrylate gelatin, methacrylate hyaluronic acid (HA), and mesoporous silica nanoparticles (GelMA/HAMA/MSN@AE), as sustained-release drug carriers for chronic wound treatment, promoted the differentiation of macrophages into the M2 phenotype.[28] Researchers created a versatile AOCuT hydrogel embedded with CuS@TA-Fe nanoparticles via Schiff base reaction. *In vivo* studies showed that this composite hydrogel effectively reduced wound inflammation and accelerated collagen deposition, epithelial tissue, and vascular regeneration.[29] Cai et al. developed curcumin-gelatin nanoparticles (CG NPs) composite carboxymethyl chitosan and sodium alginate oxide hydrogel via double crosslink without any chemical crosslink agent as a multifunctional wound healing dressing. CG NPs enhanced stability and the capacity to regulate crosslink in the injectable hydrogel, resulting in greater elasticity and rapid self-healing.[30,31] Researchers established gallium-modified gelatin nanoparticles loaded with quercetin, displaying strong anti-bacterial and inflammation properties.[32] Functionalized polylysine nanoparticles or hydrogels show great promise in biomedical research.[33,34] The positively charged polylysine exhibits significant bioactivity and versatility in various biomedical applications.[35,36] For example, cationic polylysine can interact with different anionic guest molecules through electrostatic interactions, serving as carriers for drugs and genes, antibacterial materials, coating materials, biosensors, and bioimaging agents.[37,38] Current strategies primarily concentrate on developing hydrogels for therapeutic wound applications. However, it has been recognized that the deliberate design of bioactive hydrogels, without the addition of active chemicals, can possess intrinsic biological properties. These properties include anti-inflammatory, antibacterial, anti-oxidative, pro-cell proliferation, and pro-vascularization capabilities, all of which contribute to promoting wound healing. It is challenging to develop a hydrogel dressing with an optimal combination to meet the requirements of those properties.

Considering all the reviews mentions before, we were interested in utilizing natural composite materials to fabricate hydrogel for use as a wound dressing.[39,40] Gelatin, derived from collagen, which is a significant component of the extracellular matrix (ECM), is intrinsically biodegradable and offers a variety of integrin-binding motifs, including RGD, that promote cell adhesion.[27,41] HA, also known as hyaluronate, is a versatile and polymorphic polysaccharide with extensive biological functions. It is present throughout the body, with a significant presence in the skin, where it plays a crucial role in the process of wound healing. Although gelatin and HA are natural materials and do not exhibit toxicity toward cells, they lack sufficient mechanical properties to be effectively used as wound dressings.[42] Integrating nanoparticles into hydrogels to enhance their mechanical properties represents a promising strategy to overcome this limitation.

Herein, we developed an adhesive, self-healing, and antibacterial composite hydrogel based on oxidized hyaluronic acid (Oxi-HA) and amine gelatin (Gel) hydrogel (HGel) through a Schiff-Base reaction. Lysine functionalized gelatin nanoparticles (GNPs-lysine) was composited to HGel (HGel-GNPs-lysine) via electrostatic interaction as a second crosslink to improve the mechanical properties of hydrogel (Figure 1). Since gelatin was one of the components in this hydrogel, we incorporated GNPs into the hydrogel system to create a system that was composed of natural materials, ensuring their biocompatibility with cells. Additionally, both HA and gelatin are cost-effective materials, providing an alternative solution to overcome the limitations associated with costly treatments. The effect of lysine on GNPs-lysine in the hydrogel was evaluated for enabling controllable long-term antibacterial activity against *Escherichia coli* (*E. coli*) and *Staphylococcus aureus* (*S. aureus*).

In our system, the amino residues of GNPs-lysine served as an aminoglycoside antibiotic, killing bacteria and offering high binding characteristics for negatively charged molecules through electrostatic interactions. Moreover, polylysine characteristics not only showed promising antibacterial properties but also captured multiple dangerous molecules such as pro-inflammatory cytokines, including Interleukin-1β (IL-1β) and tumor necrosis factor (TNF-α), which have been shown to prolong the inflammatory process and thereby delay healing.[33,41,43] Polylysine, due to its positive charge, easily interacts with negatively charged surfaces on various cell types, facilitating rapid attachment to polylysine substrates. Therefore, prior to conducting an *in vivo* study, the biocompatibility was assessed through *in vitro* evaluation.

Consequently, HGel and HGel-GNPs-lysine load with basic fibroblast growth factor (FGF-b) was designed for *in vivo* study to treat diabetic mice wounds. The FGF-b plays an essential role in tissue regeneration and repair. FGF-b promotes cell migration and proliferation, and also increases angiogenesis, which supports the formation of new blood vessels from existing vessels.[44] However, the therapeutic potential of FGF-b is limited due to its short *in vivo* half-life. A possible treatment for diabetic wounds could involve incorporating FGF-b into the hydrogel.[45] Finally, we examined the therapeutic impact of the hydrogel on wounds in diabetic mice (C57BL/6) using a full-thickness wound model. Subsequent assessments included the analysis of wound closure, granulation tissue thickness, collagen density, and inflammatory response.

We hypothesized that incorporating GNPs-lysine into HGel hydrogel would result in the engineering of biocompatible hydrogel. This hydrogel would possess improved mechanical strength, intrinsic bioactivity for tissue engineering, and beneficial properties such as anti-inflammation and anti-infection. Consequently, they could be extensively utilized as wound dressings, offering more effective treatment strategies that regulate and coordinate the inflammatory response at the injury site.

RESULTS AND DISCUSSION

Size and zeta potential of GNPs and GNPs-lysine

GNPs were fabricated using a two-step desolvation method, and lysine was conjugated onto the surface of GNPs using 1-ethyl-3-(3-dimethylaminopropyl) carbodiimide hydrochloride (EDC) and N-hydroxyscucinimide (NHS) to introduce a positive charge to the GNPs. Figure 2A shows the size and zeta potential (ζ) of GNPs and GNPs-lysine as measured by DLS. The average particle size of GNPs was determined

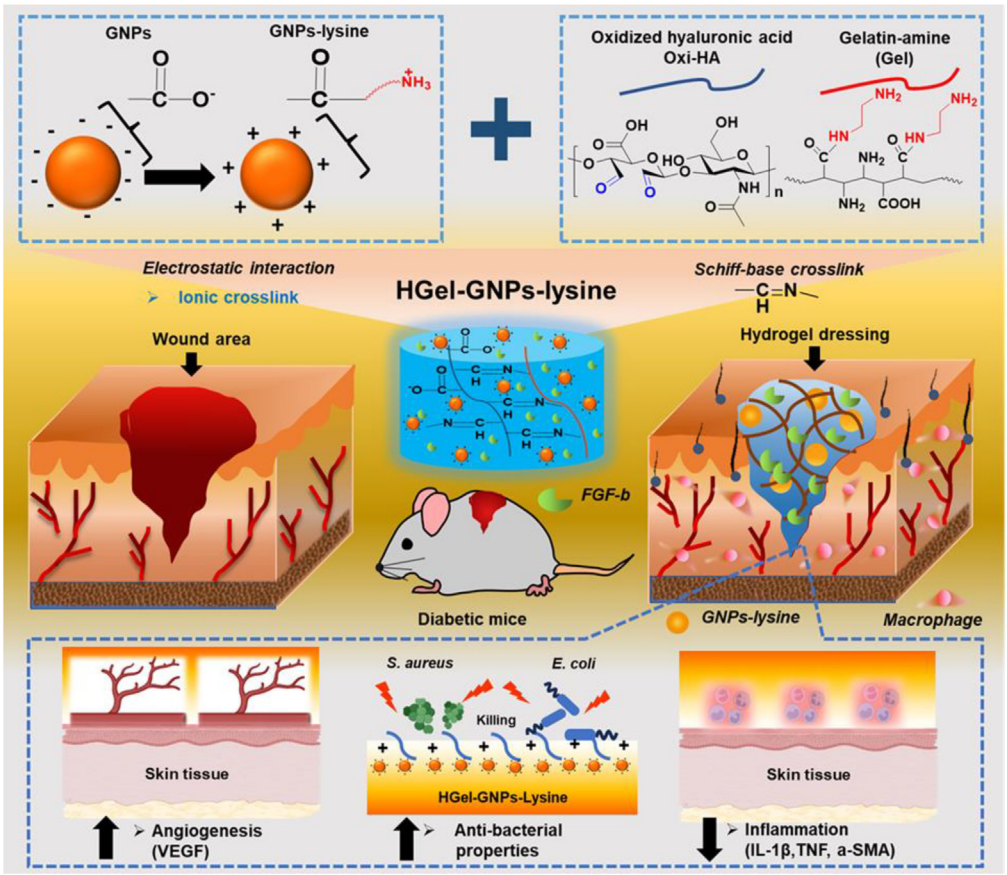

Figure 1. Schematic diagram of the synthesis process of HGel-GNPs-lysine hydrogels and their potential applications in wound repair

to be 268.5 nm, while that of GNPs-lysine was 392.5 nm, see Tables S1 and S2. The (ζ) of GNPs exhibited a negative charge of −18 mV due to the presence of carboxylic groups on the surface. Following the modification of GNPs with lysine, ζ of GNPs-lysine exhibited a positive charge of +39.7 mV due to the increased presence of amine groups on the surface, see Figures S1 and S2.

The morphology of GNPs and GNPs-lysine was characterized using a scanning electron microscope (SEM), as shown in Figure 2A, see Figure S3. GNPs exhibited a uniform, smooth, and spherical shape size of 50–70 nm. On the other hand, GNP-lysine particles were spherical and ranged from 100 to 150 nm. Additionally, the particle sizes observed in SEM images were generally smaller than those obtained through DLS measurements. These are because in DLS analysis, the particles undergo swelling, and the measurements yield a distribution of diffusion coefficients (D), which is then typically converted into a distribution of hydrodynamic diameters (*dh*). These *dh* values represent the diameters of spheres that exhibit the same *D*-values. This information deals with spherical particles, as *dh* will either be equal to or slightly larger than the actual particle diameter that was examined using the SEM technique.[46,47] The amino residues of GNPs were186 μg/mL, and the amino residues of GNPs-lysine were 805 μg/mL. [Equation: Y= (0.0022x-0.3107)/0.9895; R-squared = 0.9895].

Characterizations of Oxi-HA, Gel, and HGel hydrogel

Figure 2B presents the Fourier transform infrared spectroscopy (FTIR) spectra of gelatin, GNPs, and GNPs-lysine. Gelatin exhibited peaks at 3,300 cm^{-1}, associated with N-H stretching groups, which overlapped with the O-H vibrations of carboxylic groups. The intensities observed at 2,930, 1,645, and 1,536 cm^{-1} were attributed to CH_3, CH_2 stretching, amide I (C=O), and amide II (N–H), respectively. The GNPs- FTIR spectrum was similar to gelatin, with some shifting. For GNPs-lysine, the primary peaks occurred at 3,365, 2,944, 1,685, and 1,543 cm^{-1}. These corresponded to $–NH_2$, stretching of the primary amide comprising gelatin, $–CH_2$ stretching, amide I (C=O), and amide II (N–H), respectively, with higher intensities compared to GNPs due to L-lysine surface modification. The peaks at 1,275 and 1,050 cm^{-1} corresponded to amide III and C-O, respectively.

The HA contains adjacent hydroxyl groups, and sodium periodate ($NaIO_4$) can oxidize the o-diol structure, leading to the introduction of a double aldehyde in the HA dimmer unit. FTIR spectra of HA and its Oxi-HA are represented in Figure 2C. In the FTIR spectra of HA and Oxi-HA, the stretching vibration peaks of -OH were enhanced at 3,260 and 3,290 cm^{-1}, respectively. The spectrum of HA shows the peak at 1,045 cm^{-1} attributed to C-O-C vibration and the peaks at 1,650 and 1,410 cm^{-1} attributed to the asymmetric bending and symmetric

A

Particles	Size by DLS (nm)	Size by SEM (nm)	Zeta potential (mV)
GNPs	268.5	50-70	-18
GNPs/L-lysine	392.5	100-150	+39.7

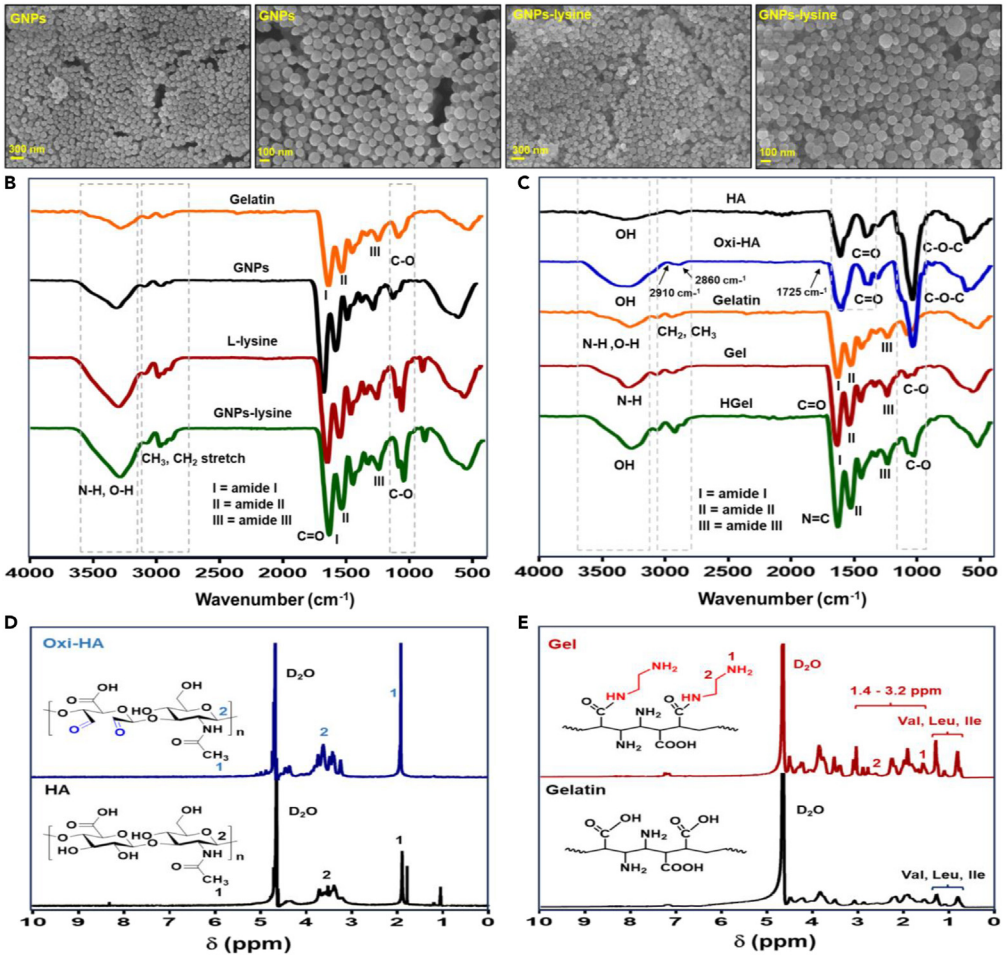

Figure 2. Characterizations of GNPs, GNPs-lysine, Oxi-HA, Gel, and HGel hydrogel

(A) Size and zeta potential of GNPs and GNPs-lysine, as measured by the DLS, and the FE-SEM images of GNPs and GNPs-lysine (scale bar:100 nm and 300 nm), see also Tables S1 and S2, Figures S1–S3.

(B) FTIR spectra of gelatin, GNPs and GNPs-lysine.

(C) FTIR spectra of HA, Oxi-HA, gelatin, Gel, and HGel hydrogel.

(D) ^{1}H-NMR of HA, Oxi-HA.

(E) ^{1}H-NMR of gelatin and Gel.

stretching of C=O groups in HA, respectively. A new band at 1,725 cm^{-1} was observed in the Oxi-HA, confirming the presence of aldehyde groups due to oxidation. It is worth noting that the spectrum of the Oxi-HA showed two absorption peaks at 2,860 to 2,910 cm^{-1}, which corresponded to the generation of the dialdehyde group. Gel was obtained by the introduction of amine groups from ethylenediamine into carboxylic groups of gelatin. In the FTIR spectrum of Gel, the stretching peak of -OH was enhanced at 3,315 cm^{-1}, associated with N-H stretching groups. The intensities observed at 2,937, 1,654, and 1,540 cm^{-1} were attributed to CH_3, CH_2 stretching, amide I (C=O), and amide II (N–H), respectively. The amino group (-NH) of Gel combines with the aldehyde group (-CHO) of Oxi-HA to form the Schiff base (-C=N), with the characteristic absorption peak of the Schiff base at 1,579 cm^{-1} for HGel hydrogel.

In the ^{1}H NMR (600 MHz, D_2O) spectrum, the absorption peak of the D_2O appears at 4.79 ppm (Figure 2D). The signals at chemical shift (δ) (ppm) 1.8 (NH-CO-CH_3), 3.2–3.9 (C*H*-O), 4.2–4.5 (O-C*H*-O), and 4.8–5.2 (hemiacetalic proton formed from aldehyde groups and neighboring hydroxyl groups), which confirmed the presence of HA and Oxi-HA (Figure 2D).[48,49] In Figure 2E, the observed resonance signals in the range of 0.9–1.6 ppm represent aliphatic protons attached to carbon atoms of valine, leucine, and isoleucine. The signals in the region 1.4–3.2 ppm

are attributed to aliphatic carbon protons of Arg, Leu, Lys, Pro, Gly, and Asp. The peaks between 3.1 and 4.5 ppm represent the resonance signals of the α-CH protons of the amino acids.[50,51]

Hydrogel formation

For the formation of each hydrogel sample, an aqueous 20% Oxi-HA solution, pH 7.4, was added to an aqueous 20% Gel in a ratio of 3:7 for gelation. Nanoparticles (10–30 mg) were added to the mixture to investigate the effect of GNPs and GNPs-lysine on the gelation time. The gelation rate of the composite hydrogel containing various amounts of GNPs and GNPs-lysine was monitored at 37°C. The gelation time for each composition was under a minute, and there were no significant differences in the gelation times among HGel, HGel-GNPs, and HGel-GNPs-lysine (Figures 3A and 3B).

Rheological properties

The rheological properties of composite hydrogels were assessed by monitoring the storage modulus (G′) as a function of angular frequency at 37°C (Figure 3C). As the amount of GNPs and GNPs-lysine increased, the G′ value consistently increased with the nanoparticle concentration. HGel-GNPs-lysine (30 mg) exhibited the highest G′ (~3,800 Pa), followed by HGel-GNPs (30 mg; ~2,500 Pa) and H-Gel (1,750 Pa). The G′ value hydrogel increased as a result of the addition of GNPs and GNPs-lysine. These are because the nanoparticles acted as nanoscale crosslink points evenly distributed through the hydrogel network, and the flexible polymer chains between the nanoparticles have similar chain lengths, allowing for efficient stress dissipation within the hydrogels.[52] In the case of GNPs-lysine crosslink, the excess amino groups in GNPs-lysine may crosslink with the unreacted aldehyde groups in Oxi-HA. Additionally, the negatively charged carboxylic groups of the HA chains can interact ionically with the positively charged GNPs-lysine, creating a secondary physical crosslink. Besides, the introduction of GNPs into HGel improves the modulus properties, likely through interactions between the hydrogen bonding of COOH from HA and unreacted NH_2 groups of Gel chains with GNPs, resulting in double crosslink via hydrogen bonding.[53]

Swelling, biodegradation, and morphology of the hydrogels

The hydrogel equilibrium swelling ratios were measured at pH 7.4°C and 37°C over a 24 h (Figure 3D). The capacity of hydrogels to absorb water, as reflected in their swelling ratios, is crucial for their biological activity. All hydrogels showed an increase in swelling ratios with prolonged incubation. However, the incorporation of GNPs or GNPs-lysine into the composite hydrogel resulted in a reduction in the swelling ratio. After 24 h, the swelling ratio of HGel increased to 700, notably higher than that of HGel-GNPs and HGel-GNPs-lysine. These could be attributed to the lower crosslink of hydrogels, which allows for greater branching of polymer chains, facilitating easier expansion in water. HGel-GNPs and HGel-GNPs-lysine had particles occupying the structural space within the hydrogel system, limiting their water absorption capacity. The hydrogel network experienced reduced water uptake. The density of double crosslink between polymer chains and nanoparticles plays a role in determining the properties of the hydrogel, resulting in a decrease in the swelling ratio. A higher crosslink density leads to a lower swelling ratio.[54–57]

Weight loss of hydrogels was monitored in Hyclone phosphate buffer saline (PBS) at 37°C over time. The weight of HGel drastically decreased within 24 h and continued to reduce until day 14, resulting in 100% degradation (Figure 3E). The degradation rate of HGel-GNPs-lysine-30 mg was slightly lower, with approximately 90% of the initial weight remaining at day 14. The degradation rates of HGel-GNPs-lysine-20 mg and 10 mg were slightly lower than that of the 30 mg composition, with the weights remaining at 85% and 83%, respectively. HGel-GNPs showed a higher degradation rate compared with HGel-GNPs-lysine for all compositions (30, 20, and 10 mg), with the weights remaining at 70%, 65%, and 25%, respectively. The graphs corresponding to HGel-GNPs or HGel-GNPs-lysine showed lower degradation rates compared with the native HGel hydrogel. These findings indicated that the degradation rate of hydrogels depends on the extent of crosslink, where a higher number of crosslink results in less weight loss of the hydrogel.

Figure 3F displays the cross-sectional SEM images of lyophilized HGel, HGel-GNPs, and HGel-GNPs-lysine hydrogels. The hydrogels demonstrated interconnected and uniformly distributed porous structures. The pore size of HGel ranged from approximately 50 to 90 μm, while the pore sizes of HGel-GNPs and HGel-GNPs-lysine were smaller, measuring around 30 to 70 μm and 10 to 25 μm, respectively. The reduced pore diameter indicated an increase in crosslink density.[56] In HGel-GNPs and HGel-GNPs-lysine, the matrix surrounding the pores contained GNPs and GNPs-lysine, resulting in a rough surface. In contrast, the matrix around the pores of the HGel hydrogel exhibited a smooth surface. This observation confirms the successful embedding of GNPs and GNPs-lysine into the hydrogel.

The morphology of degrading hydrogels was investigated. SEM images of freeze-dried hydrogels indicated that HGel-GNPs and HGel-GNPs-lysine retained their porous structures after seven days of incubation. In the absence of nanoparticles, the hydrogel porous structure collapsed. Moreover, in contrast to the native hydrogel, GNPs, and GNPs-lysine were distinctly observable. These results suggest that the introduction of nanoparticles can markedly enhance the mechanical properties of the hydrogel and decelerate its degradation.

Cell viability and proliferation

Live/dead assay fluorescence pictures of GNPs and GNPs-lysine from day 1 to day 7 incubation are shown in Figure 4A. Green fluorescence indicates living cells, while red fluorescence indicates dead cells. Compared to the control group, the cells that grew together with GNPs and GNPs-lysine had higher density, and nearly no red fluorescence could be seen in the field of vision. Figure 4B indicated the absorbance significantly increased when culturing human adipose-derived stem cell (hASC) with GNPs and GNPs-lysine compared to the control group

A

Conditions					
	Concentration of oxidized HA (%)	Concentration of gelatin amine (%)	Ratios	GNPs (mg)	Gelation time (min)
1	20	20	3/7	-	~1
2	20	20	3/7	10	~1
3	20	20	3/7	20	~1
4	20	20	3/7	30	~1
	Concentration of oxidized HA (%)	Concentration of gelatin amine (%)	Ratios	GNPs-lysine (mg)	Gelation time (min)
5	20	20	3/7	10	~1
6	20	20	3/7	20	~1
7	20	20	3/7	30	~1

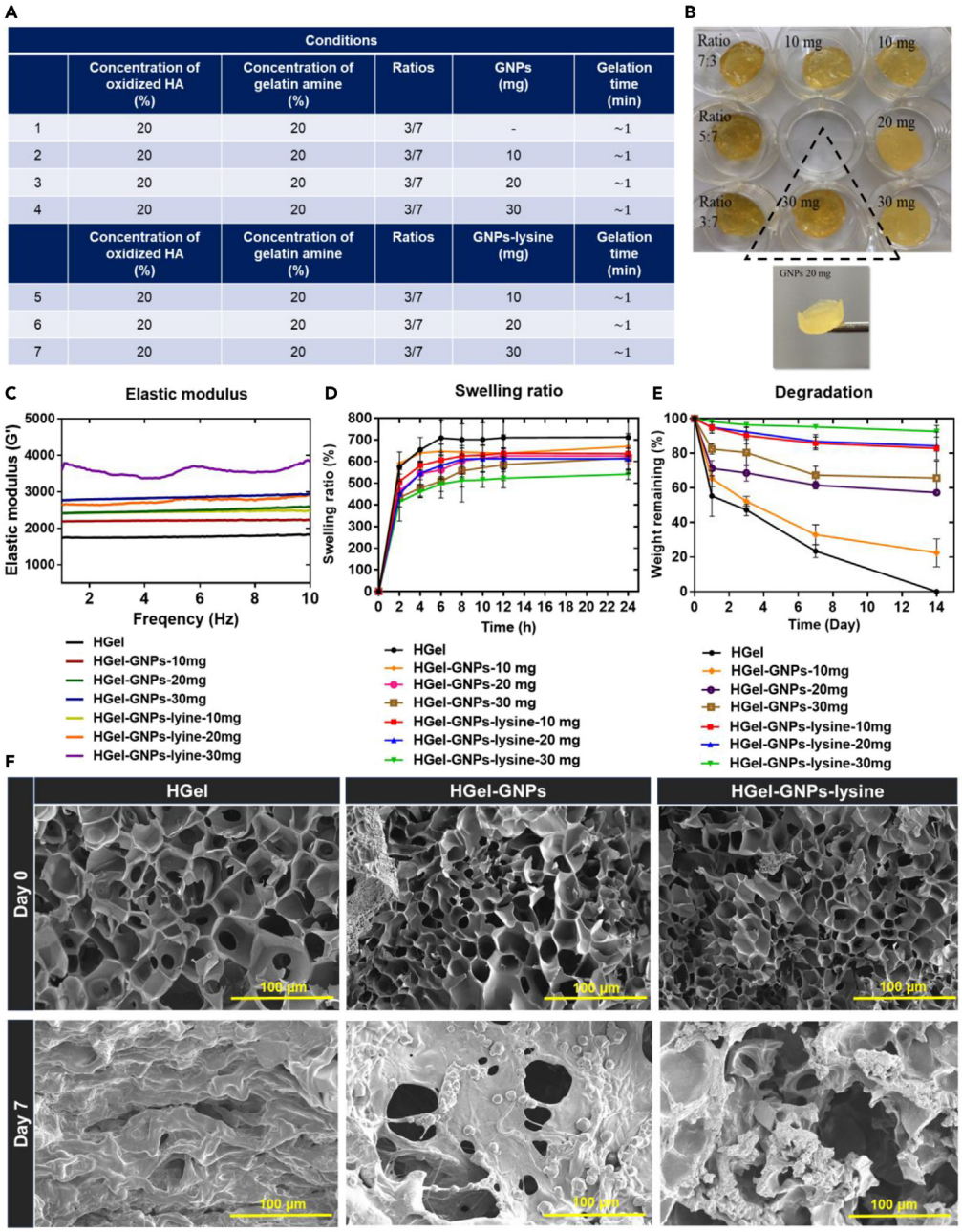

Figure 3. Hydrogel formation and characterizations

(A) Optimized conditions for the preparation of HGel, HGel-GNPs, and HGel-GNPs-lysine hydrogels.

(B) Images of HGel hydrogels with various concentrations of GNPs and GNPs-lysine after gelation.

(C) Frequency dependence of storage modulus (G').

(D) Swelling ratio.

(E) Percentage of weight remaining.

(F) SEM images of cross-section HGel, HGel-GNPs (30 mg), and HGel-GNPs-lysine (30 mg) after lyophilization (day 0) and after degradation at day 7; scale bar: 100 μm.

(without nanoparticles) at day 3 and day 7 (****: $p < 0.0001$). To assess biocompatibility and favorable microenvironment for supporting the proliferation of hASCs, we employed hydrogels, including HGel, HGel-GNPs, and HGel-GNPs-lysine, for culturing hASCs for seven days. Matrigel, known for its robust promotion of cell proliferation and differentiation in 3D cell culture, was utilized as a positive control in this study (Figure 4C). The cell proliferation in all hydrogel groups steadily increased from day 1 to day 7. The cell numbers of hASCs treated with HGel,

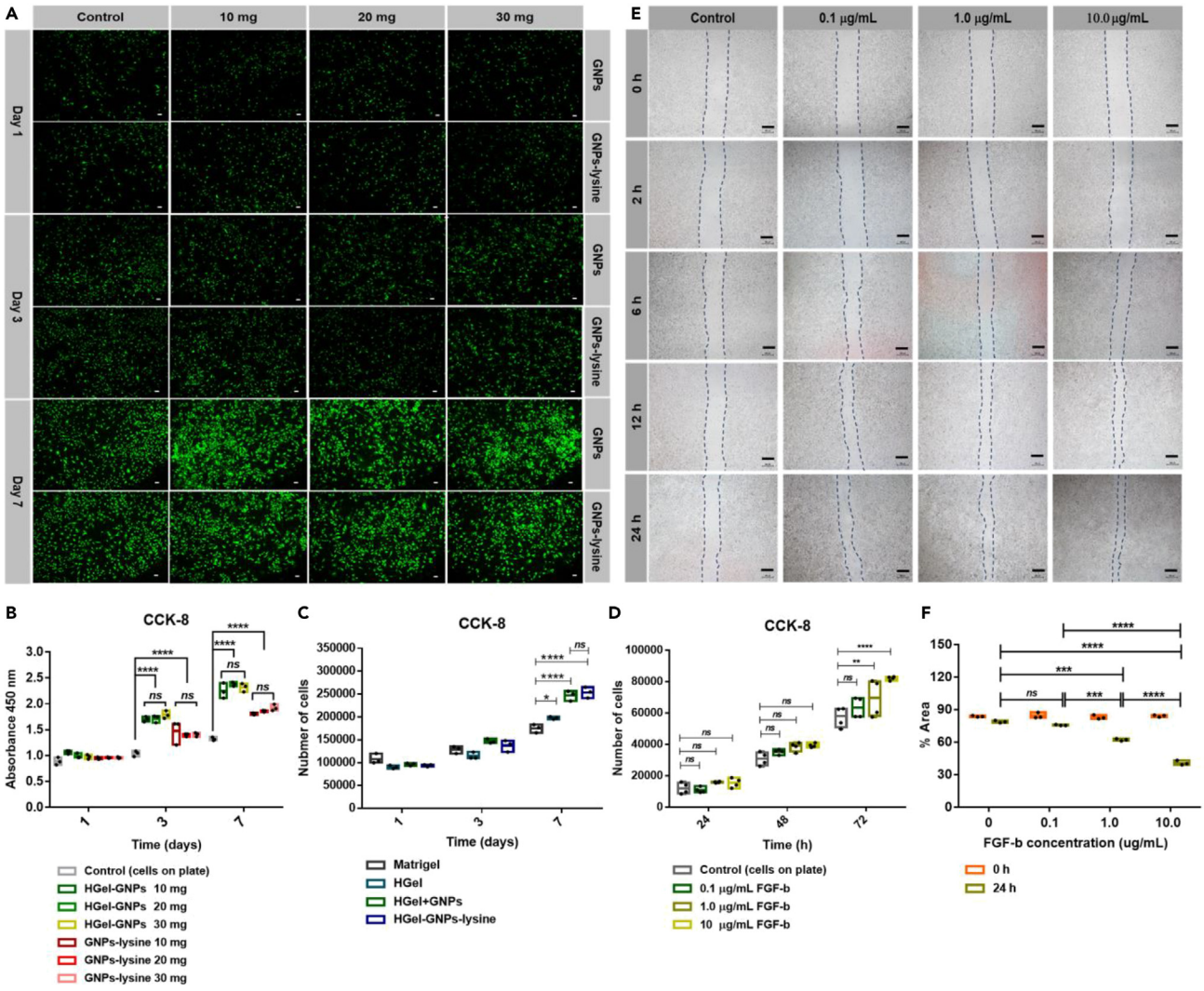

Figure 4. Biocompatibility evaluation of GNPs and GNPs-lysine and hydrogels

(A) Live/dead assay of hASCs treated with GNPs and GNPs-lysine at different concentrations for 7 days; scale bar: 50 μm.

(B) Cell proliferation in hASCs treated with GNPs and GNPs-lysine for 7 days. Results are presented as mean ± SD, and analyzed using two-way ANOVA with Tukey's test for multiple comparisons. Number of hASC culture with nanoparticles (n) = 3 per group, *p < 0.05, **p < 0.01, ***p < 0.001, ****p < 0.0001; ns indicates p > 0.05.

(C) Cell proliferation in hASCs treated with different hydrogels (Matrigel, HGel, HGel-GNPs, and HGel-GNPs-lysine; 30 mg) for 7 days. Results are presented as mean ± SD, and analyzed using two-way ANOVA with Tukey's test for multiple comparisons. Number of hASC cultured with hydrogels (n) = 3 per group, *p < 0.05, **p < 0.01, ***p < 0.001, ****p < 0.0001; ns indicates p > 0.05.

(D) The proliferation of hASCs treated with different concentrations of FGF-b for 72 h. Results are presented as mean ± SD, and analyzed using two-way ANOVA with Tukey's test for multiple comparisons. Number of hASC treated with FGF-b (n) = 3 per group, *p < 0.05, **p < 0.01, ***p < 0.001, ****p < 0.0001; ns indicates p > 0.05.

(E) Representative photographs of the effect of FGF-b on macrophage migration at 0 h, 2 h, 6 h, 12 h, and 24 h following the treatments with control, 0.1 μg/mL, 1.0 μg/mL and 10.0 μg/mL FGF-b; scale bar: 250 μm.

(F) Quantification of the remaining scratch wound area percentage at 0 h, 2 h, 6 h, 12 h, and 24 h. Results are presented as mean ± SD, and analyzed using two-way ANOVA with Tukey's test for multiple comparisons. Number of scratch wound area (n) = 3 per group, *p < 0.05, **p < 0.01, ***p < 0.001, ****p < 0.0001; ns indicates p > 0.05.

HGel-GNPs, and HGel-GNPs-lysine showed no significant difference compared to those treated with Matrigel on day 1 and day 3. HGel-GNPs and HGel-GNPs-lysine hydrogels significantly promoted hASCs proliferation compared to HGel hydrogel and Matrigel at day 7. However, there was no significant difference between hASCs treated with HGel-GNPs and HGel-GNPs-lysine on day 7. These findings suggest that the hydrogel system we designed, specifically HGel-GNPs-lysine, did not exert harmful effects on hASCs. These results were consistent with the study that utilized polylysine to promote the growth of mesenchymal stem cells (MSCs). MSCs cultured with polylysine exhibited a

faster growth rate and upregulated expression of stemness markers.[37] Lysine can serve as an attachment factor that enhances cell adherence, as there is an electrostatic interaction between the positive charge on the lysine molecule and the negative charge on the cell membrane. It demonstrated that HGel-GNPs-lysine provides a favorable microenvironment for hASCs proliferation.

FGF-b plays a crucial role in tissue regeneration and repair processes by facilitating angiogenesis and stimulating cell migration and proliferation.[44,45] In our study, we investigated the impact of varying concentrations of FGF-b on hASCs proliferation. As illustrated in Figure 4D, the proliferation of hASCs was heightened with an increase in FGF-b concentration, ranging from 0.1 μg/mL to 10.0 μg/mL. After 72 h, a significant enhancement in hASCs proliferation was observed upon treatment with 1.0 μg/mL and 10.0 μg/mL of FGF-b, suggesting that FGF-b has the capacity to promote cell proliferation.

Macrophages play a crucial role in the inflammatory response during wound healing, performing diverse functions such as infection defense, inflammation regulation, clearance of apoptotic cells, and support for tissue regeneration after injury.[58,59] Recent studies highlight their presence in healing wounds and their influence on each stage of the repair process. Collective cell migration is a key feature of wound healing, involving various events such as fibrin clot decomposition, ECM interactions, and wound contraction. In our investigation, a scratch wound was induced in a fibroblast monolayer to assess the impact of FGF-b on cell migration. As depicted in Figures 4E and 4F, cell migration exhibited varying degrees of enhancement following exposure to different concentrations of FGF-b for 6 to 24 h. Macrophages (Raw 264.7) treated with FGF-b at concentrations of 0.1, 1.0, and 10.0 μg/mL exhibited a decrease in the remaining wound area by 75%, 62%, and 42%, respectively, compared to cells not subjected to FGF-b treatment after 24 h. Consequently, FGF-b at a concentration of 10.0 μg/mL was chosen for further *in vivo* experiments due to its efficacy in promoting cells proliferation and migration.

Anti-bacterial potential of hydrogels

The role of preventing infections and expediting wound healing is crucially played by the antibacterial properties of hydrogel. Qualitative methods were employed to investigate the antibacterial effects of the hydrogels against *E. coli* and *S. aureus*, with initial concentrations of 1.4×10^6 CFU/mL and 1.0×10^6 CFU/mL, respectively. As depicted in Figures 5A1 and 5B1, the uneven sizes of the hydrogel were observed due to the hydrolysis reaction of the Schiff base crosslink under physiological conditions. HGel and HGel-lysine were directly applied to the surface of bacterial culture dishes to prevent mass loss during transfer. The remaining H_2O from the Schiff base crosslink hydrogel formation initiated the hydrolysis reaction at the beginning of the experiment, resulting in uneven hydrogel sizes. It is important to note that HGel and HGel-GNPs-lysine were composed of the same volume of hydrogel for both *E. coli* and *S. aureus* experiments. There was a slightly higher mass of hydrogel in HGel-GNPs-lysine due to the additional presence of GNPs-lysine compared to HGel. However, there was no discernible impact on the antibacterial properties of the hydrogel for both *E. coli* and *S. aureus*.

Results from the zone of inhibition (ZOI) experiment, depicted in Figures 5A1, 5A2, 5B1, and 5B2, revealed clear inhibition zones for HGel, HGel-GNPs, and HGel-GNPs-lysine hydrogels, with varying sizes of antibacterial circles. HGel-GNPs-lysine demonstrated the largest inhibition zone, whereas HGel exhibited the smallest for *S. aureus*, with no significant differences observed between HGel and HGel-GNPs. Furthermore, in the case of the *E. coli* antibacterial test, HGel-GNPs-lysine displayed a significantly larger inhibition area compared to HGel-GNPs and HGel, respectively. The antibacterial activity of the hydrogels resulted in bacterial aggregation and morphological destruction, as illustrated in Figures 5A3, 5A4, 5B3, and 5B4.

The optical density (OD) of the bacterial solution was further assessed at various time intervals (Figures 5C and 5D), with PBS and 75% ethanol serving as positive and negative controls, respectively. After 2 h of treatment, a notable reduction in OD value was evident in the hydrogel-treated groups compared to the positive control group for both *E. coli* and *S. aureus*. After 24 h of treatment, the observed difference persisted, surpassing the antibacterial efficacy of the negative control groups. These emphasized the heightened effectiveness of the HGel-GNPs-lysine in combating bacterial activity. Within the hydrogel treated groups, HGel-GNPs-lysine demonstrated the most robust antibacterial activity, surpassing not only the negative control but also the HGel and HGel-GNPs groups. The HGel-GNPs-lysine hydrogel consistently showed significantly improved antibacterial potential, aligning with the outcomes observed through the ZOI method.

The results indicated that HGel-GNPs-lysine hydrogel exhibited antibacterial effects by altering the membrane permeability of bacteria and through electrostatic interactions between $-NH^{3+}$ groups and functional groups on the bacterial membrane surface.[43] Several $-NH_2$ groups exhibited positive charge effectively, inhibiting or even eliminating bacterial growth.[60,61] The reason for the limited inhibitory zone observed with HGel is that the free amine groups on the gelatin were crosslink with Oxi-HA, which resulted in the retention of a small number of free amine groups. In contrast, HGel-GNPs and HGel-GNPs-lysine had a higher concentration of free amine groups compared to HGel alone. The presence of lysine groups from GNPs-lysine and the partially free amine residues on GNPs could enhance the antibacterial properties more effectively than HGel. Thus, these results demonstrated that HGel-GNPs-lysine could exert antibacterial effects due to its excellent antioxidant properties, which could further enhance the process of wound healing.

In vivo wound healing test in a diabetic mouse model

We evaluated the wound healing ability of the hydrogels immobilized FGF-b using a diabetic C57BL/6 mice model. The body weight measurement was carried out for 14 days, and the weight remained constant in every experiment group, see Figure S4. Wound contraction was monitored by photographing the wounds at predetermined time points (day 1, 4, 7, 10, and 14) (Figure 6A). As shown in Figure 6B, the wounds of mice treated with hydrogels exhibited significantly faster healing compared to the control group (saline) and the FGF-b group. On day 1, all groups had similar wound sizes, around 8 mm in diameter. On day 4, the wounds covered with hydrogels started to heal significantly faster (HGel, 64.4%; HGel-GNPs-lysine-30mg, 55.2%) than those treated with saline (85.7%) and slightly faster than those treated with FGF-b (70.6%).

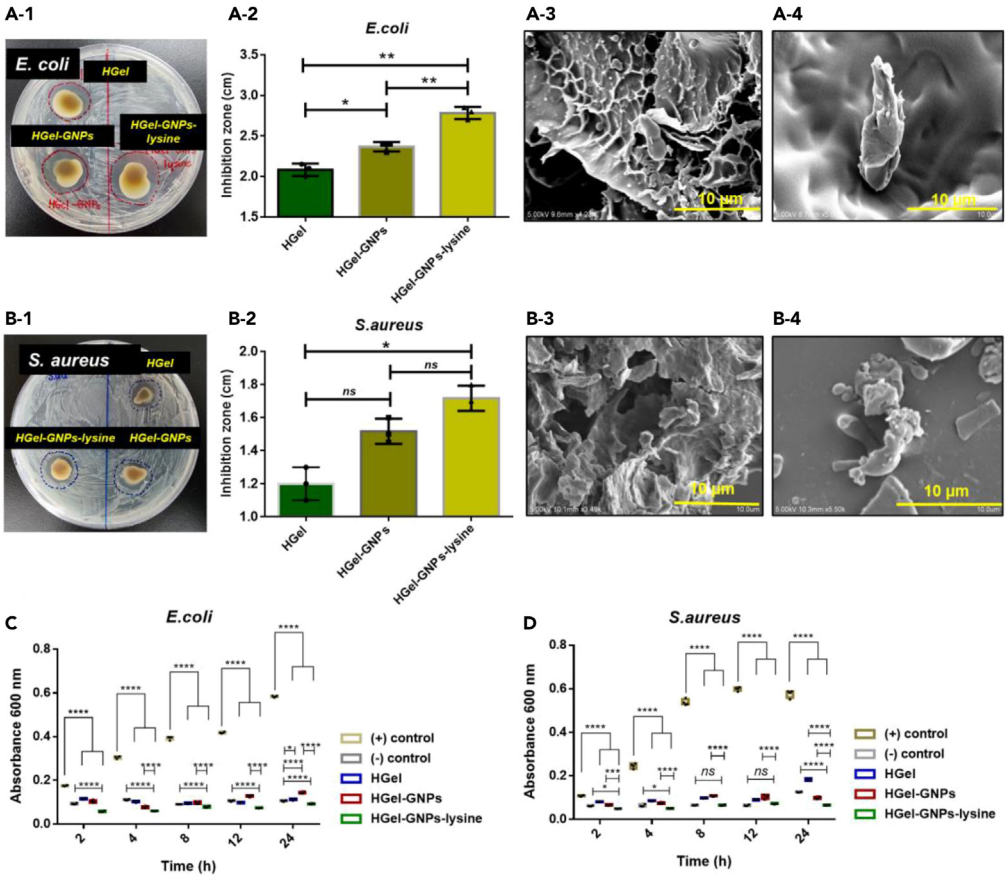

Figure 5. *In vitro* antibacterial activity of hydrogels against *E. coli* and *S. aureus*

(A1 and A2) The inhibition zone of HGel, HGel-GNPs, and HGel-GNPs-lysine against *E. coli* for 12 h. Results are presented as mean ± SD, and analyzed using one-way ANOVA with Tukey's test for multiple comparisons. Number of hydrogels (n) = 3 per group, *p < 0.05, **p < 0.01, ***p < 0.001, ****p < 0.0001; ns indicates p > 0.05.

(B1 and B2) The inhibition zone of HGel, HGel-GNPs, and HGel-GNPs-lysine against *S. aureus* for 12 h. Results are presented as mean ± SD, and analyzed using one-way ANOVA with Tukey's test for multiple comparisons. Number of hydrogels (n) = 3, *p < 0.05, **p < 0.01, ***p < 0.001, ****p < 0.0001; ns indicates p > 0.05.

(A3 and A4) SEM images of *E. coli* adhered to HGel and HGel-GNPs (30 mg); scale bar: 10 μm.

(B3 and B4) SEM images of *S. aureus* adhered to HGel and HGel-GNPs (30 mg); scale bar: 10 μm.

(C and D) Growth curves of *E. coli* and *S. aureus* after incubation with saline (control, +), 75% ethanol (control, −), HGel, and HGel-GNPs-lysine for 24 h. Results are presented as mean ± SD, and analyzed using two-way ANOVA with Tukey's test for multiple comparisons. Number of hydrogels (n) = 3, *p < 0.05, **p < 0.01, ***p < 0.001, ****p < 0.0001; ns indicates p > 0.05.

From day 7 onwards, the gap between the hydrogel-treated wounds (HGel, 47.1%; HGel-GNPs-lysine-30mg, 35.2%) and the FGF-b group (61.2%) continued to widen, Figure 6C.

As depicted in Figure 6C, by the 14th day, wounds treated with hydrogels had nearly completed healing, while the control group still exhibited approximately 12% of the wound area remaining unhealed. Additionally, for a hydrogel to serve as an effective wound dressing, it should possess suitable adhesive strength and healing properties. Figure 6D illustrates the adherence of hydrogel to wounds, ears, or tails, indicating that HGel-GNPs-lysine displayed noteworthy adhesive properties. To support these observations, we conducted an experiment evaluating the adhesive properties of the hydrogels, utilizing porcine skin as a substitute for human skin (Figures 6E–6G). HGel-GNPs-lysine-30 mg exhibited the highest lap shear strength, measuring 8,000 kPa, significantly surpassing HGel-GNPs and HGel. On the other hand, there was no significant difference in the lap shear strength between HGel and HGel-GNPs-10 mg. These could be attributed to the highly cationic nature of HGel-GNPs-lysine, which contributes to strong adhesion to skin tissue, resulting in remarkably enhanced adhesion strength.[43,62,63]

Histological evaluation

The process of wound healing is a complex physiological process enclosing various stages such as hemostasis, inflammation, migration, proliferation, and remodeling.[64–66] In-depth exploration of the impact of hydrogels on wound healing involved histological analyses to examine the regenerating and normal tissues in mice. Hematoxylin and eosin staining (H&E staining) and Masson trichrome staining (MT staining) were utilized to evaluate the effects of wound healing on days 7 and 14, as depicted in Figures 7A and 7B.

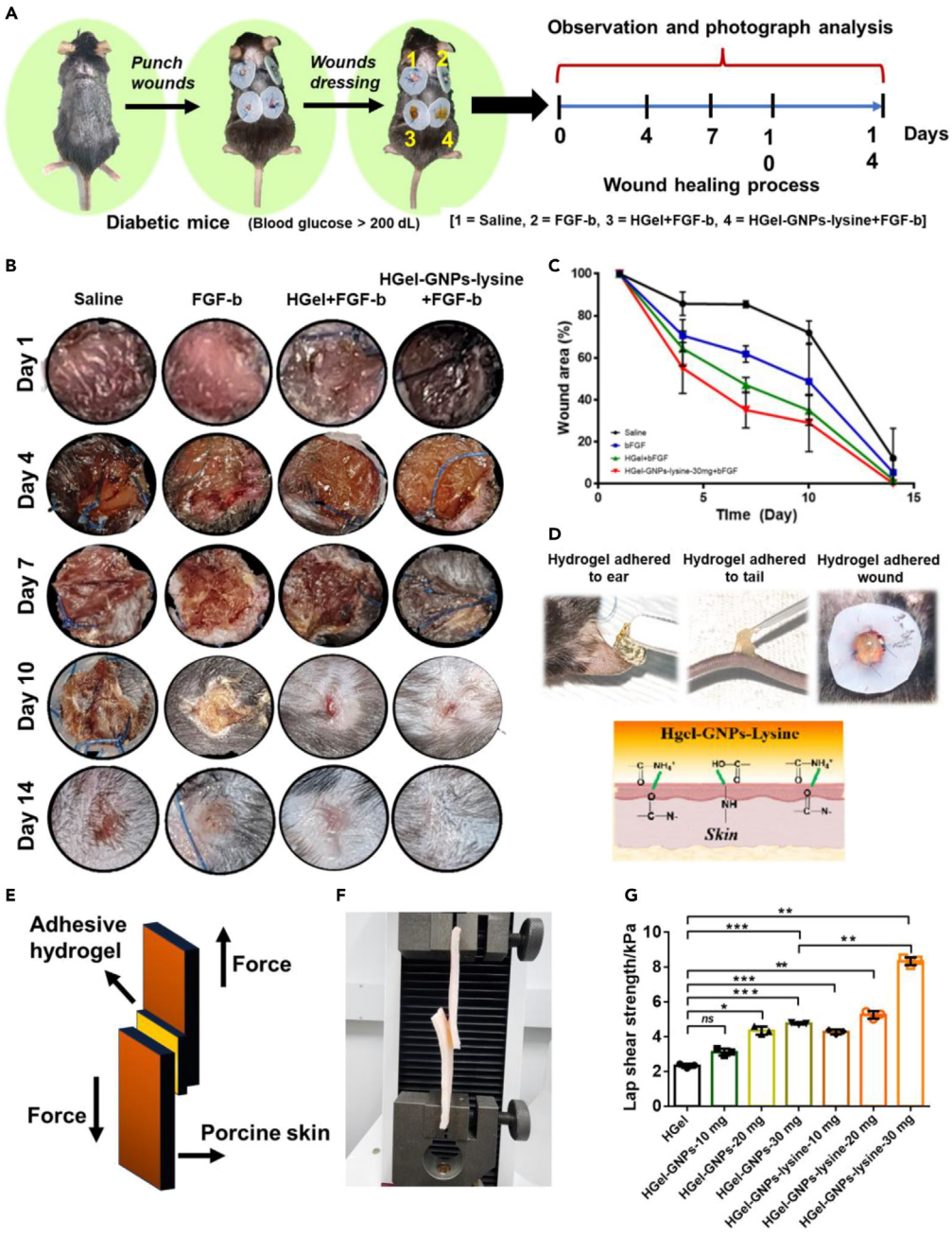

Figure 6. *In vivo* performance of hydrogels promoting diabetic wound healing

(A) Schematic of the construction and treatment of wounds in a diabetic mouse model with HGel and HGel-GNPs-lysine hydrogels.

(B) Representative images of wounds treated with control (saline), FGF-b, HGel+FGF-b, and HGel-GNPs-lysine+FGF-b at different time points.

(C) Wound area at different time points.

(D) Images of hydrogels adhered to mouse skin.

(E and F) Schematic presentation of the lap shear test.

(G) The lap shear strength to porcine skin. Results are presented as mean ± SD, and analyzed using one-way ANOVA with Tukey's test for multiple comparisons. Number of hydrogels (n) = 3, *p < 0.05, **p < 0.01, ***p < 0.001, ****p < 0.0001; ns indicates p > 0.05.

Epidermal thickness was quantitatively analyzed (Figure 7C), revealing a significant decrease in the FGF-b, HGel+FGF-b, and HGel-GNPs-lysine + FGF-b groups compared to the control group at day 7 and 14. However, there was no significant difference in Epidermal thickness between the control and FGF-b treatment groups at day 7. These suggested a reduction in scar tissue formation, as indicated by the red arrow

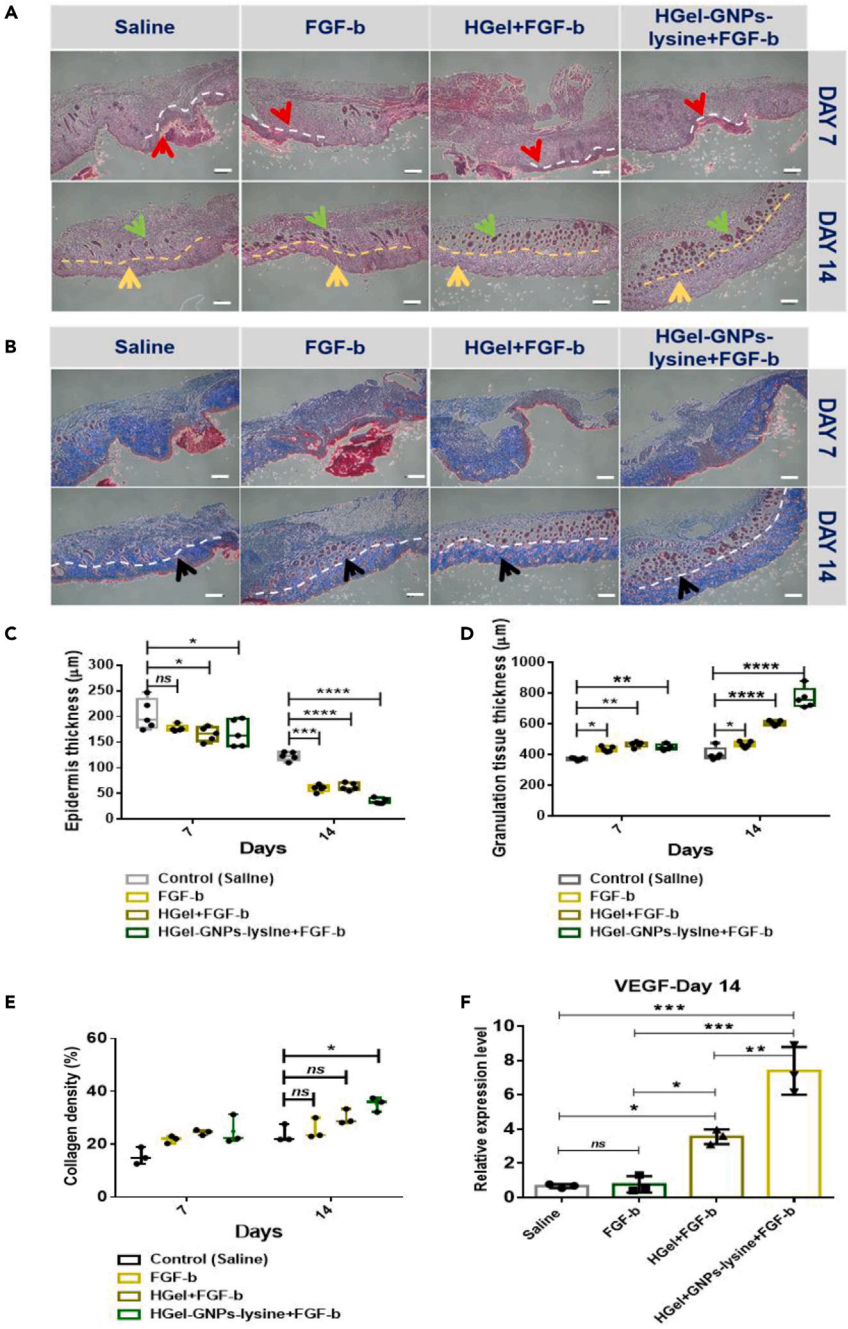

Figure 7. Histological analysis of wound tissues after treatment with saline (control), FGF-b, HGel+FGF-b, and HGel-GNPs-lysine+FGF-b at day 7 and day 14

(A) H&E staining images; scale bar: 200 μm.

(B) MT staining images; scale bar: 200 μm.

(C) Epidermis thickness. Results are presented as mean ± SD, and analyzed using two-way ANOVA with Tukey's test for multiple comparisons. Number of tissues (n) = 5, *p < 0.05, **p < 0.01, ***p < 0.001, ****p < 0.0001; ns indicates p > 0.05.

(D) Granulation tissue thickness. Results are presented as mean ± SD, and analyzed using two-way ANOVA with Tukey's test for multiple comparisons. Number of tissues (n) = 5, *p < 0.05, **p < 0.01, ***p < 0.001, ****p < 0.0001; ns indicates p > 0.05.

(E) Collagen density. Results are presented as mean ± SD, and analyzed using two-way ANOVA with Tukey's test for multiple comparisons. Number of tissues (n) = 3, *p < 0.05, **p < 0.01, ***p < 0.001, ****p < 0.0001; ns indicates p > 0.05.

Figure 7. *Continued*

(F) Quantitative PCR analysis of VEGF gene expression in wound tissues treated with saline, FGF-b, HGel+FGF-b, and HGel-GNPs-lysine+FGF-b, expressed relative to the mRNA levels of glyceraldehyde 3-phosphate dehydrogenase (GAPDH) at day 14. Results are presented as mean ± SD, and analyzed using one-way ANOVA with Tukey's test for multiple comparisons. Number of tissues (n) = 3, *$p < 0.05$, **$p < 0.01$, ***$p < 0.001$, ****$p < 0.0001$; ns indicates $p > 0.05$.

in Figure 7A. Granulation tissue, comprising accumulated ECM, fibroblasts, and various cells, plays an essential role in the process of wound healing. Variations in granulation tissue thickness were observed among the groups (yellow arrow, Figure 7A). On day 7, the granulation tissue in all hydrogel treatment groups was significantly higher than the control group. Moreover, on day 14, the granulation tissue in the HGel-GNPs-lysine+FGF-b group exhibited an approximately 700 μm greater thickness compared to the HGel+FGF-b, FGF-b, and control groups (Figure 7D). The *in vivo* study indicated that the HGel-GNPs-lysine+FGF-b dressing improved wound healing by promoting the thickness of granulation tissue. Furthermore, the number of hair follicle regeneration in the HGel-GNPs-lysine+FGF-b group was higher than in other groups, Figure 7A (green arrow).

The total collagen level in the granulation tissue, a key indicator of wound healing, was evaluated through the analysis of MT staining. Collagen density, represented by the blue-stained regions, were observed in all groups and at all time points (black arrow, Figure 7B). The hydrogel groups, especially HGel-GNPs+FGF-b, showed higher collagen deposition on both day 7 and day 14. The control group displayed less collagen deposition. Quantitative analysis results shown in Figure 7E further revealed a significant increase in collagen density in the HGel-GNPs-lysine+FGF-b group compared with the control groups on day 14 ($p \leq 0.05$). In addition, FGF-b and HGel+FGF-b treatment groups showed slightly higher collagen density than the control group, but there was no significant difference on day 7 and day 14.

Collagen is the main component of the dermis and provides elasticity and toughness to the skin. The balance between collagen synthesis and degradation is crucial in wound healing.[29] The elevated level of collagen content in the wounds treated with HGel-GNPs-lysine+FGF-b indicated that the introduction of FGF-b into the hydrogel accelerated the biological process of wound healing by upregulating collagen production and accurately regulating collagen content throughout the entire healing stage. Moreover, the incorporation of FGF-b could promote angiogenesis in the wound.

Angiogenesis, the formation of new blood vessels from pre-existing vessels, is a critical element in the repair mechanism. In the skin, vascular endothelial growth factor (VEGF) is a highly influential proangiogenic growth factor. The level of VEGF within a wound plays a substantial role in determining the pace and effectiveness of the healing process. FGF-b is involved in angiogenesis and has been found at a high level in acute wounds to promote tissue remodeling. In our investigations, we assessed the expression of VEGF in the wound tissue following treatment with FGF-b and FGF-b deposited in hydrogels on day 14 (Figure 7F).

In vivo studies have demonstrated that the application of FGF-b accelerates the process of tissue repair. FGF-b could be administered through hydrogel for tissue regeneration. There was a significant increase in VEGF expression in HGel-GNPs-lysine+FGF-b and HGel+FGF-b, respectively, compared with the control group. According to the hydrolysis of Schiff base hydrogel in wound healing, it could be advantageous, as controlled hydrolysis can release any encapsulated therapeutic agents or drugs within the hydrogel. This addition to the wound healing process provides a sustained and controlled release of FGF-b. Besides, there was no difference in VEGF expression between the control and FGF-b treatment groups. These could be explained by the short half-life of FGF-b *in vivo*. These results indicated that HGel and HGel-GNPs-lysine administered FGF-b to promote angiogenesis in wound tissue.

Quantitative PCR

We examined the expression of cytokine genes during wound healing using quantitative PCR, Figure 8. The expression levels of α-smooth muscle actin (α-SMA), collagen 1 alpha 1 (COL1a1), and collagen 3 alpha 1 (COL3a1) genes were compared between groups at each time point. We observed a significant decrease in COL3a1 levels in the FGF-b and hydrogel treatment groups compared with the control group at 7 days ($p < 0.05$) and day 14 ($p < 0.01$). COL1a1 expression was downregulated in both hydrogel treatment groups at days 7 and day 14 ($p < 0.01$). However, COL1a1 expression levels did not significantly differ between the FGF-b and the control group at day 7. In addition, we found that the expression of α-SMA was significantly decreased in the hydrogel treatment groups at day 7 and day 14 compared with the control group ($p < 0.01$). However, α-SMA expression was slightly higher in the FGF-b group compared to hydrogel treatment groups at day 14, but it was significantly lower than the control group ($p < 0.05$).

TNF-α is released by vascular endothelial cells, keratinocytes, and fibroblasts in the injured area, initiating the inflammatory phase and promoting the recruitment of inflammatory leukocytes. Downregulation of TNF-α expression was observed in the FGF-b and hydrogel treatment groups, although the difference was not statistically significant when compared to the control samples.

We further analyzed the expression levels of IL-1β, another inflammatory cytokine gene. The expression level of IL-1β in the HGel+FGF-b, HGel-GNPs+FGF-b treatment groups was significantly lower compared with the control group ($p < 0.01$) at day 7. In addition, the expression of IL-1β was not significantly different for FGF-b and hydrogel treatment groups compared to the control group at day 14. These results suggest that the proposed hydrogel system might be able to reduce inflammation during the early stages of the wound healing process.

Cluster of differentiation 68 (CD68) is a marker for monocytes and macrophages, commonly found near wounds. Its expression is highly associated with inflammation, and CD68 expression decreases as inflammation is reduced. We found that the expression of CD68 decreased in all treatment groups compared with the control group ($p < 0.01$) at day 14. Nevertheless, there was no significant difference in CD68 expression between the FGF-b and control groups at day 7. In contrast, significantly elevated gene expressions were detected in HGel+FGF-b and HGel-GNPs-lysine+FGF-b compared to the control group ($p < 0.01$)

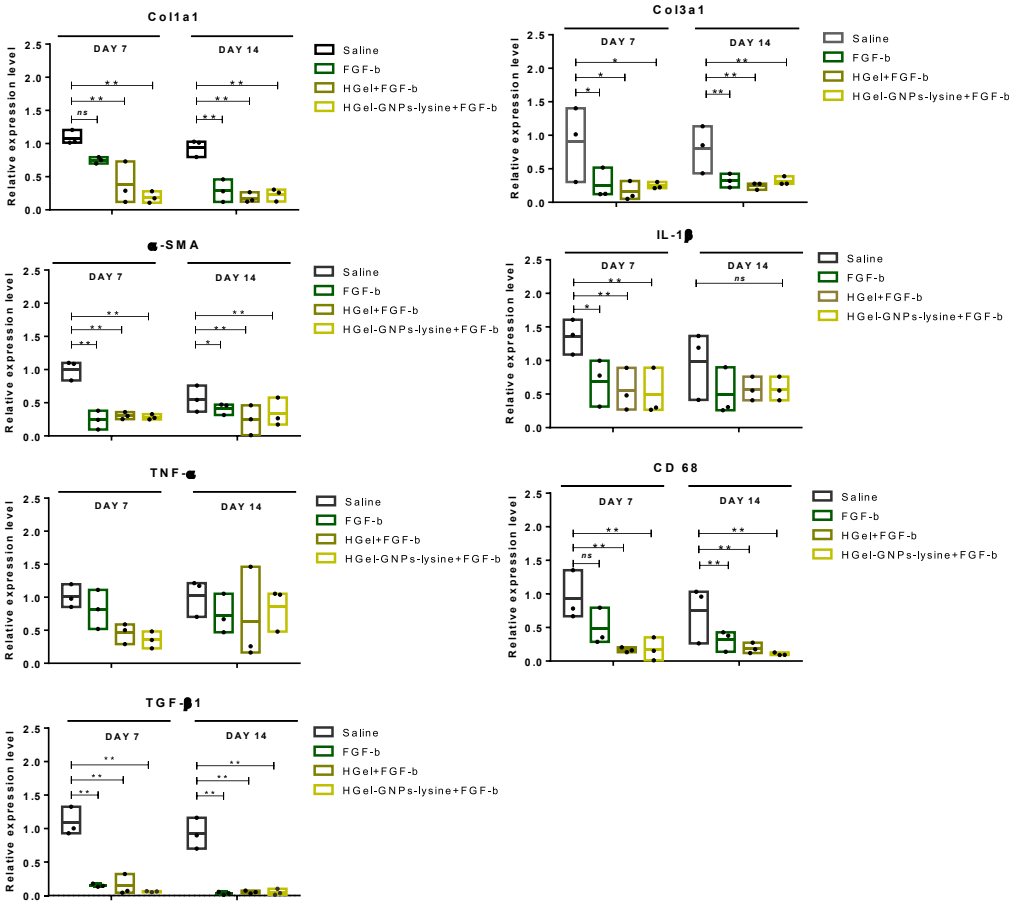

Figure 8. Quantitative PCR analysis of gene expression in wound tissues treated with saline, FGF-b, HGel+FGF-b, and HGel-GNPs-lysine+FGF-b, expressed relative to the mRNA levels of GAPDH at 7 and 14 days

Results are presented as mean ± SD, and analyzed using two-way ANOVA with Tukey's test for multiple comparisons. Number of tissues (n) = 3, *$p < 0.05$, **$p < 0.01$, ***$p < 0.001$, ****$p < 0.0001$; ns indicates $p > 0.05$.

Transforming growth factor beta 1 (TGF-β1) is a cytokine involved in fibrosis and affects the differentiation of fibroblasts into myofibroblasts. At day 7 and day 14, the expression levels of TGF-β were significantly lower in all treatment groups compared with the control group ($p < 0.01$). According to these findings, our HGel-GNPs-lysine hydrogel had a relatively good curative effect, anti-inflammation, and angiogenesis as a wound dressing.

There are numerous reasons diabetic wounds become chronic. In brief, diabetic wounds are more susceptible to infection, have lower antimicrobial capacity, and lack adequate blood supply. Our newly introduced hydrogel specifically targets these features of diabetic wounds to promote tissue regeneration. Our results indicate that the GNP-lysine composited hydrogel, loaded with FGF dressing, has demonstrated promising results in expediting the initial stages of wound healing. Diabetic wounds often experience delays in the inflammatory phase, which is when the body responds to injury. If a topical dressing material can enhance and expedite this inflammatory phase, it sets a positive quality for the entire healing process in diabetic wounds.[67] Furthermore, the positively charged surface of GNP-lysine enhances its antimicrobial properties, a crucial factor in addressing chronic wounds in diabetes. Diabetic wounds are more likely to infections due to poor blood circulation, which can further hinder healing. The positive charge present on the surface of GNP-lysine enables the hydrogel to effectively eliminate both gram-positive and gram-negative bacteria. These antimicrobial properties can play a pivotal role in expediting the healing process. Additionally, incorporating advanced wound care techniques with growth factors can stimulate tissue regeneration. These approaches significantly accelerate the formation of new blood vessels and tissues, which are essential for closing the wound. These are particularly significant for diabetic wounds that lack adequate blood circulation. Composing growth factors that promote vessel and tissue generation on the GNP-lysine hydrogel will play an essential role in diabetic wound management.[68,69]

In conclusion, a comprehensive approach that addresses multiple aspects of diabetic wound healing demonstrates therapeutic benefits within a few weeks. It is all about effectively addressing the unique challenges presented by diabetic wounds and promoting a faster, more efficient healing response.

Limitations of the study

In this study, we created a multifunctional hydrogel with accelerated wound healing and antibacterial properties. The hydrogel was designed using a dual crosslink mechanism involving Schiff base and electrostatic interactions, enabling the incorporation of adjustable properties such as swelling ratio, degradation rate, and adhesive strength. The positively charged GNPs-lysine served as a second crosslink agent, enhancing the adhesion between the hydrogel and the tissue. The hydrogel could form *in situ* within a short period and adhere firmly to the wound surface without the need for additional adhesive agents. *E. coli* and *S. aureus* bacteria were efficiently killed by the hydrogel owing to the positively charged surface of GNPs-lysine. HGel-GNPs-lysine+FGF-b hydrogel dressings significantly improved granulation tissue formation and collagen density in a diabetic mice wound model. According to gene expression analyses, the proposed hydrogel system dramatically reduced inflammation and encouraged angiogenesis. HGel-GNPs-lysine+FGF-b hydrogels demonstrated multifunctional qualities, such as increased healing and antimicrobial activities, making them a promising substitute for the treatment of diabetic wounds. Despite the positive aspects of their wound healing performance and relatively low-cost materials, this study has certain limitations due to the use of hydrogel compositions based on natural polymers. As a result, the mechanical properties of the hydrogels are relatively low, and the performance of each batch varies significantly. Another issue with Schiff base hydrogels is their limited ability to absorb large amounts of fluid, making them unsuitable for very wet wounds, which could lead to maceration and infection due to the reversible imine bonds with changes in pH value. Given the growing demand for higher-performance dressings, there has been increased interest in the development of hydrogel dressings with multifunctional properties, such as antibacterial ability, excellent mechanical properties, biodegradability, responsiveness, and injectability, in the field of wound dressings in recent years. Therefore, this study could be further enhanced to improve certain characteristics, such as controlling moisture around the wound, ensuring ease of changing and removing dressings with adequate mechanical properties, and alleviating wound pain. This research presented a simple approach to developing a low-cost, antibacterial, and anti-inflammatory hydrogel that could effectively promote the wound healing process. However, there are possibilities for further development and improvement to meet the demands for more effective and versatile wound dressings.

STAR★METHODS

Detailed methods are provided in the online version of this paper and include the following:

- KEY RESOURCES TABLE
- RESOURCE AVAILABILITY
  - Lead contact
  - Materials availability
  - Data and code availability
- EXPERIMENTAL MODEL AND STUDY PARTICIPANT DETAILS
  - Diabetic mice model
  - hASC culture
  - Raw 264.7 culture
  - Microbe strains
- METHOD DETAILS
  - Preparation of gelatin GNPs through a two-step desolvation method
  - GNPs-lysine preparation
  - Determination of nanoparticle size distribution
  - Preparation of oxidized hyaluronic acid (Oxi-HA)
  - Preparation of amine gelatin (Gel)
  - Characterizations of Oxi-HA, Gel, GNPs, and GNPs-lysine
  - Hydrogel fabrication and gelation time measurement
  - Swelling and degradation properties
  - Morphology
  - Rheological properties
  - Measurement of adhesion ability
  - Biocompatibility and cell migration
  - Antibacterial ability test
  - *In vivo* wound healing assay
  - Histology evaluation
  - Reverse transcription followed by quantitative polymerase chain reaction
- QUANTIFICATION AND STATISTICAL ANALYSIS

SUPPLEMENTAL INFORMATION

Supplemental information can be found online at https://doi.org/10.1016/j.isci.2024.108860.

ACKNOWLEDGMENTS

This research was supported by a grant of Korean Cell-Based Artificial Blood Project funded by the Korean government (The Ministry of Science and ICT, The Ministry of Trade, Industry and Energy, the Ministry of Health and Welfare, the Ministry of Food and Drug Safety) (grant number: HX23C1734) and the Chung-Ang University Research Grants in 2022.

AUTHOR CONTRIBUTIONS

S.K.: methodology, design and synthesis materials, formal analysis, conduct animal experiment, writing – original draft, review & editing. A.C.: synthesis and characterization of materials, conduct animal experiment. I.Y.A.: conduct animal experiment. W.J.K.: conduct animal experiment. T.H.B.: conduct animal experiment. S.H.K.: conceptualization, methodology, supervision, project administration. H.P.: conceptualization, methodology, supervision, project administration, funding acquisition.

DECLARATION OF INTERESTS

The authors declare no conflict of interests.

Received: July 24, 2023
Revised: November 11, 2023
Accepted: January 8, 2024
Published: January 11, 2024

REFERENCES

1. Han, G., and Ceilley, R. (2017). Chronic Wound Healing: A Review of Current Management and Treatments. Adv. Ther. *34*, 599–610.
2. Fan, F., Saha, S., and Hanjaya-Putra, D. (2021). Biomimetic Hydrogels to Promote Wound Healing. Front. Bioeng. Biotechnol. *9*, 718377.
3. Flynn, K., Mahmoud, N.N., Sharifi, S., Gould, L.J., and Mahmoudi, M. (2023). Chronic Wound Healing Models. ACS Pharmacol. Transl. Sci. *6*, 783–801.
4. Firlar, I., Altunbek, M., McCarthy, C., Ramalingam, M., and Camci-Unal, G. (2022). Functional Hydrogels for Treatment of Chronic Wounds. Gels *8*, 127.
5. Wu, S., Wu, X., Wang, X., and Su, J. (2023). Hydrogels for bone organoid construction: From a materiobiological perspective. J. Mater. Sci. Technol. *136*, 21–31.
6. Yu, F., Geng, D., Kuang, Z., Huang, S., Cheng, Y., Chen, Y., Leng, F., Bei, Y., Zhao, Y., Tang, Q., et al. (2022). Sequentially releasing self-healing hydrogel fabricated with TGFβ3-microspheres and bFGF to facilitate rat alveolar bone defect repair. Asian J. Pharm. Sci. *17*, 425–434.
7. Huang, C., Dong, L., Zhao, B., Lu, Y., Huang, S., Yuan, Z., Luo, G., Xu, Y., and Qian, W. (2022). Anti-inflammatory hydrogel dressings and skin wound healing. Clin. Transl. Med. *12*, e1094.
8. Zhang, W., Liu, W., Long, L., He, S., Wang, Z., Liu, Y., Yang, L., Chen, N., Hu, C., and Wang, Y. (2023). Responsive multifunctional hydrogels emulating the chronic wounds healing cascade for skin repair. J. Contr. Release *354*, 821–834.
9. Tavakoli, S., and Klar, A.S. (2020). Advanced Hydrogels as Wound Dressings. Biomolecules *10*, 1169.
10. Huang, S., Hong, X., Zhao, M., Liu, N., Liu, H., Zhao, J., Shao, L., Xue, W., Zhang, H., Zhu, P., and Guo, R. (2022). Nanocomposite hydrogels for biomedical applications. Bioeng. transl. med. *7*, e10315.
11. Hong, C., Chung, H., Lee, G., Kim, C., Kim, D., Oh, S.J., Kim, S.-H., and Lee, K. (2023). Hydrogel/Nanofiber composite wound dressing optimized for skin layer regeneration through the mechanotransduction-Based microcellular environment. Appl. Bio Mater. *6*, 1774–1786.
12. Wahid, F., Zhao, X.-J., Jia, S.-R., Bai, H., and Zhong, C. (2020). Nanocomposite hydrogels as multifunctional systems for biomedical applications: Current state and perspectives. Compos. B Eng. *200*, 108208.
13. Zhao, H., Liu, M., Zhang, Y., Yin, J., and Pei, R. (2020). Nanocomposite hydrogels for tissue engineering applications. Nanoscale *12*, 14976–14995.
14. Pardo, A., Gómez-Florit, M., Barbosa, S., Taboada, P., Domingues, R.M.A., and Gomes, M.E. (2021). Magnetic Nanocomposite Hydrogels for Tissue Engineering: Design Concepts and Remote Actuation Strategies to Control Cell Fate. ACS Nano *15*, 175–209.
15. Shalaby, M.A., Anwar, M.M., and Saeed, H. (2022). Nanomaterials for application in wound Healing: current state-of-the-art and future perspectives. J. Polym. Res. *29*, 91.
16. Naskar, A., and Kim, K.-S. (2020). Recent Advances in Nanomaterial-Based Wound-Healing Therapeutics. Pharmaceutics *12*, 499.
17. Qin, W., Wu, Y., Liu, J., Yuan, X., and Gao, J. (2022). Comprehensive Review of the Application of Nanoparticles in Diabetic Wound Healing: Therapeutic Potential and Future Perspectives. Int. J. Nanomed. *17*, 6007–6029.
18. Fei, R., George, J.T., Park, J., and Grunlan, M.A. (2012). Thermoresponsive nanocomposite double network hydrogels. Soft Matter *8*, 481–487.
19. Xue, L., Deng, T., Guo, R., Peng, L., Guo, J., Tang, F., Lin, J., Jiang, S., Lu, H., Liu, X., and Deng, L. (2022). A Composite Hydrogel Containing Mesoporous Silica Nanoparticles Loaded With Artemisia argyi Extract for Improving Chronic Wound Healing. Front. Bioeng. Biotechnol. *10*, 825339.
20. Bernal-Chávez, S.A., Alcalá-Alcalá, S., Cerecedo, D., and Ganem-Rondero, A. (2020). Platelet lysate-loaded PLGA nanoparticles in a thermo-responsive hydrogel intended for the treatment of wounds. Eur. J. Pharmaceut. Sci. *146*, 105231.
21. Zhou, X., Chen, T., Ma, T., Yan, L., Wei, H., Liu, S., Dai, Z., Xie, Z., Deng, J., Tao, S., et al. (2023). CuS@TA-Fe Nanoparticle-Doped Multifunctional Hydrogel with Peroxide-Like Properties and Photothermal Properties for Synergistic Antimicrobial Repair of Infected Wounds. Adv. Healthcare Mater. *12*, 2301206.
22. Cui, G., Guo, X., Su, P., Zhang, T., Guan, J., and Wang, C. (2023). Mussel-inspired nanoparticle composite hydrogels for hemostasis and wound healing. Front. Chem. *11*, 1154788.
23. Dai, X., Guo, Q., Zhao, Y., Zhang, P., Zhang, T., Zhang, X., and Li, C. (2016). Functional silver nanoparticle as a benign antimicrobial agent that eradicates antibiotic-resistant bacteria and promotes wound healing. ACS Appl. Mater. Interfaces *8*, 25798–25807.
24. Wang, X., Lv, F., Li, T., Han, Y., Yi, Z., Liu, M., Chang, J., and Wu, C. (2017). Electrospun micropatterned nanocomposites incorporated with Cu2S nanoflowers for skin tumor therapy and wound healing. ACS Nano *11*, 11337–11349.
25. Wang, S., Yan, C., Zhang, X., Shi, D., Chi, L., Luo, G., and Deng, J. (2018). Antimicrobial peptide modification enhances the gene delivery and bactericidal efficiency of gold nanoparticles for accelerating diabetic wound healing. Biomater. Sci. *6*, 2757–2772.
26. Dam, P., Celik, M., Ustun, M., Saha, S., Saha, C., Kacar, E.A., Kugu, S., Karagulle, E.N., Tasoglu, S., Buyukserin, F., et al. (2023). Wound healing strategies based on nanoparticles incorporated in hydrogel wound patches. RSC Adv. *13*, 21345–21364.
27. Yi, X., He, J., Wei, X., Li, H., Liu, X., and Cheng, F. (2023). A polyphenol and ε-polylysine functionalized bacterial cellulose/PVA

multifunctional hydrogel for wound healing. Int. J. Biol. *247*, 125663.
28. Zengin, A., Castro, J.P.O., Habibovic, P., and van Rijt, S.H. (2021). Injectable, self-healing mesoporous silica nanocomposite hydrogels with improved mechanical properties. Nanoscale *13*, 1144–1154.
29. Chen, Y., Zheng, K., Niu, L., Zhang, Y., Liu, Y., Wang, C., and Chu, F. (2019). Highly mechanical properties nanocomposite hydrogels with biorenewable lignin nanoparticles. Int. J. Biol. *128*, 414–420.
30. Cai, X., He, Y., Cai, L., Zhan, J., Li, Q., Zhong, S., Hou, H., Wang, W., and Qiu, X. (2023). An injectable elastic hydrogel crosslinked with curcumin–gelatin nanoparticles as a multifunctional dressing for the rapid repair of bacterially infected wounds. Biomater. Sci. *11*, 3227–3240.
31. Hajati Ziabari, A., Asadi Heris, M., Mohammad Doodmani, S., Jahandideh, A., Koorehpaz, K., and Mohammadi, R. (2022). Cinnamon Nanoparticles Loaded on Chitosan-Gelatin Nanoparticles Enhanced Burn Wound Healing in Diabetic Foot Ulcers in Rats. Int. J. Low. Extrem. Wounds. https://doi.org/10.1177/15347346221101245.
32. Yang, N., Shi, N., Yao, Z., Liu, H., and Guo, W. (2023). Gallium-modified gelatin nanoparticles loaded with quercetin promote skin wound healing via the regulation of bacterial proliferation and macrophage polarization. Front. Bioeng. Biotechnol. *11*, 1124944.
33. Mou, C., Wang, X., Teng, J., Xie, Z., and Zheng, M. (2022). Injectable self-healing hydrogel fabricated from antibacterial carbon dots and ϵ-polylysine for promoting bacteria-infected wound healing. J. Nanobiotechnol. *20*, 368.
34. Zarrintaj, P., Ghorbani, S., Barani, M., Singh Chauhan, N.P., Khodadadi Yazdi, M., Saeb, M.R., Ramsey, J.D., Hamblin, M.R., Mozafari, M., and Mostafavi, E. (2022). Polylysine for skin regeneration: A review of recent advances and future perspectives. Bioeng. Transl. Med. *7*, e10261.
35. Fürsatz, M., Skog, M., Sivlér, P., Palm, E., Aronsson, C., Skallberg, A., Greczynski, G., Khalaf, H., Bengtsson, T., and Aili, D. (2018). Functionalization of bacterial cellulose wound dressings with the antimicrobial peptide ε-poly-L-Lysine. Biomed. Mater. *13*, 025014.
36. Mazia, D., Schatten, G., and Sale, W. (1975). Adhesion of cells to surfaces coated with polylysine. Applications to electron microscopy. J. Cell Biol. *66*, 198–200.
37. Heo, J.S., Kim, H.O., Song, S.Y., Lew, D.H., Choi, Y., and Kim, S. (2016). Poly-L-lysine prevents senescence and augments growth in culturing mesenchymal stem cells ex vivo. BioMed Res. Int. *2016*, 8196078.
38. Zhu, H., Liu, R., Shang, Y., and Sun, L. (2023). Polylysine complexes and their biomedical applications. Eng. Regen. *4*, 20–27.
39. Augustine, R., Zahid, A.A., Hasan, A., Dalvi, Y.B., and Jacob, J. (2021). Cerium Oxide Nanoparticle-Loaded Gelatin Methacryloyl Hydrogel Wound-Healing Patch with Free Radical Scavenging Activity. ACS Biomater. Sci. Eng. *7*, 279–290.
40. Ndlovu, S.P., Ngece, K., Alven, S., and Aderibigbe, B.A. (2021). Gelatin-Based Hybrid Scaffolds: Promising Wound Dressings. Polymers *13*, 2959.
41. Teng, L., Shao, Z.W., He, Y.S., Lu, J.Y., Zou, D.R., Feng, C.L., and Dong, C.M. (2022). A Glycosylated and Catechol-crosslinked ε-Polylysine Hydrogel: Simple Preparation and Excellent Wound Hemostasis and Healing Properties. Chin. J. Polym. Sci. *40*, 1110–1119.
42. Frenkel, J.S. (2014). The role of hyaluronan in wound healing. Int. Wound J. *11*, 159–163.
43. Liu, S., Liu, X., Ren, Y., Wang, P., Pu, Y., Yang, R., Wang, X., Tan, X., Ye, Z., Maurizot, V., and Chi, B. (2020). Mussel-Inspired Dual-Cross-linking Hyaluronic Acid/ε-Polylysine Hydrogel with Self-Healing and Antibacterial Properties for Wound Healing. ACS Appl. Mater. Interfaces *12*, 27876–27888.
44. Wei, L., Tan, J., Li, L., Wang, H., Liu, S., Chen, J., Weng, Y., and Liu, T. (2022). Chitosan/Alginate Hydrogel Dressing Loaded FGF/VE-Cadherin to Accelerate Full-Thickness Skin Regeneration and More Normal Skin Repairs. Int. J. Mol. Sci. *23*, 1249.
45. Wylie, R.G., and Shoichet, M.S. (2011). Three-Dimensional Spatial Patterning of Proteins in Hydrogels. Biomacromolecules *12*, 3789–3796.
46. Fissan, H., Ristig, S., Kaminski, H., Asbach, C., and Epple, M. (2014). Comparison of different characterization methods for nanoparticle dispersions before and after aerosolization. Anal. Methods *6*, 7324–7334.
47. Bootz, A., Vogel, V., Schubert, D., and Kreuter, J. (2004). Comparison of scanning electron microscopy, dynamic light scattering and analytical ultracentrifugation for the sizing of poly(butyl cyanoacrylate) nanoparticles. Eur. J. Pharm. Biopharm. *57*, 369–375.
48. Li, N.-N., Fu, C.-P., and Zhang, L.-M. (2014). Using casein and oxidized hyaluronic acid to form biocompatible composite hydrogels for controlled drug release. Mater. Sci. Eng. C *36*, 287–293.
49. Li, L., Wang, N., Jin, X., Deng, R., Nie, S., Sun, L., Wu, Q., Wei, Y., and Gong, C. (2014). Biodegradable and injectable in situ cross-linking chitosan-hyaluronic acid based hydrogels for postoperative adhesion prevention. Biomaterials *35*, 3903–3917.
50. Poveda-Reyes, S., Moulisova, V., Sanmartín-Masiá, E., Quintanilla-Sierra, L., Salmerón-Sánchez, M., and Ferrer, G.G. (2016). Extracellular Matrix-Inspired Gelatin/Hyaluronic Acid Injectable Hydrogels. Macromol. Biosci. *16*, 1311–1324.
51. Amonpattaratkit, P., Khunmanee, S., Kim, D.H., and Park, H. (2017). Synthesis and Characterization of Gelatin-Based Crosslinkers for the Fabrication of Superabsorbent Hydrogels. Materials *10*, 826.
52. Li, Y., Liu, C., Tan, Y., Xu, K., Lu, C., and Wang, P. (2014). In situ hydrogel constructed by starch-based nanoparticles via a Schiff base reaction. Carbohydr. Polym. *110*, 87–94.
53. Gupta, B., Tummalapalli, M., Deopura, B.L., and Alam, M.S. (2014). Preparation and characterization of in-situ crosslinked pectin–gelatin hydrogels. Carbohydr. Polym. *106*, 312–318.
54. Chen, H., Xing, X., Tan, H., Jia, Y., Zhou, T., Chen, Y., Ling, Z., and Hu, X. (2017). Covalently antibacterial alginate-chitosan hydrogel dressing integrated gelatin microspheres containing tetracycline hydrochloride for wound healing. Mater. Sci. Eng. C *70*, 287–295.
55. Fan, M., Ma, Y., Tan, H., Jia, Y., Zou, S., Guo, S., Zhao, M., Huang, H., Ling, Z., Chen, Y., and Hu, X. (2017). Covalent and injectable chitosan-chondroitin sulfate hydrogels embedded with chitosan microspheres for drug delivery and tissue engineering. Mater. Sci. Eng. C *71*, 67–74.
56. Kamoun, E.A. (2016). N-succinyl chitosan–dialdehyde starch hybrid hydrogels for biomedical application. J. Adv. Res. *7*, 69–77.
57. Zhang, L., Li, K., Xiao, W., Zheng, L., Xiao, Y., Fan, H., and Zhang, X. (2011). Preparation of collagen–chondroitin sulfate–hyaluronic acid hybrid hydrogel scaffolds and cell compatibility in vitro. Carbohydr. Polym. *84*, 118–125.
58. Koh, T.J., and DiPietro, L.A. (2011). Inflammation and wound healing: the role of the macrophage. Expet Rev. Mol. Med. *13*, e23.
59. Krzyszczyk, P., Schloss, R., Palmer, A., and Berthiaume, F. (2018). The Role of Macrophages in Acute and Chronic Wound Healing and Interventions to Promote Pro-wound Healing Phenotypes. Front. Physiol. *9*, 419.
60. Patel, D.K., Ganguly, K., Hexiu, J., Dutta, S.D., Patil, T.V., and Lim, K.-T. (2022). Functionalized chitosan/spherical nanocellulose-based hydrogel with superior antibacterial efficiency for wound healing. Carbohydr. Polym. *284*, 119202.
61. Fu, Y., Zhang, J., Wang, Y., Li, J., Bao, J., Xu, X., Zhang, C., Li, Y., Wu, H., and Gu, Z. (2021). Reduced polydopamine nanoparticles incorporated oxidized dextran/chitosan hybrid hydrogels with enhanced antioxidative and antibacterial properties for accelerated wound healing. Carbohydr. Polym. *257*, 117598.
62. Valencia, C., Valencia, Y., and Grande Tovar, C.D. (2020). Synthesis and Application of a Cationic Polyamine as Yankee Dryer Coating Agent for the Tissue Paper-Making Process. Polymers *12*, 173.
63. Hu, H., Zhai, X., Li, W., Ji, S., Dong, W., Chen, W., Wei, W., and Lu, Z. (2022). A photo-triggering double cross-linked adhesive, antibacterial, and biocompatible hydrogel for wound healing. iScience *25*, 104619.
64. Vizely, K., Wagner, K.T., Mandla, S., Gustafson, D., Fish, J.E., and Radisic, M. (2023). Angiopoietin-1 derived peptide hydrogel promotes molecular hallmarks of regeneration and wound healing in dermal fibroblasts. iScience *26*, 105984.
65. Attasgah, R.B., Velasco-Rodríguez, B., Pardo, A., Fernández-Vega, J., Arellano-Galindo, L., Rosales-Rivera, L.C., Prieto, G., Barbosa, S., Soltero, J.F.A., Mahmoudi, M., and Taboada, P. (2022). Development of functional hybrid scaffolds for wound healing applications. iScience *25*, 104019.
66. Hu, J.-J., Yu, X.-Z., Zhang, S.-Q., Zhang, Y.-X., Chen, X.-L., Long, Z.-J., Hu, H.-Z., Xie, D.H., Zhang, W.-H., Chen, J.-X., and Zhang, Q. (2023). Hydrogel with ROS scavenging effect encapsulates BR@Zn-BTB nanoparticles for accelerating diabetic mice wound healing via multimodal therapy. iScience *26*, 106775.

67. Burgess, J.L., Wyant, W.A., Abdo Abujamra, B., Kirsner, R.S., and Jozic, I. (2021). Diabetic Wound-Healing Science. Medicina *57*, 1072.

68. Gao, D., Zhang, Y., Bowers, D.T., Liu, W., and Ma, M. (2021). Functional hydrogels for diabetic wound management. APL Bioeng. *5*, 031503.

69. Spampinato, S.F., Caruso, G.I., De Pasquale, R., Sortino, M.A., and Merlo, S. (2020). The Treatment of Impaired Wound Healing in Diabetes: Looking among Old Drugs. Pharmaceuticals *13*, 60.

70. Sutthiwanjampa, C., Shin, B.H., Ryu, N.E., Kang, S.H., Heo, C.Y., and Park, H. (2022). Assessment of human adipose-derived stem cell on surface-modified silicone implant to reduce capsular contracture formation. Bioeng. Transl. Med. *7*, e10260.

71. Coester, C.J., Langer, K., van Briesen, H., and Kreuter, J. (2000). Gelatin nanoparticles by two step desolvation-a new preparation method, surface modifications and cell uptake. J. Microencapsul. *17*, 187–193.

72. Pandit, A.H., Mazumdar, N., and Ahmad, S. (2019). Periodate oxidized hyaluronic acid-based hydrogel scaffolds for tissue engineering applications. Int. J. Biol. Macromol. *137*, 853–869.

73. Furman, B.L. (2021). Streptozotocin-Induced Diabetic Models in Mice and Rats. Curr. Protoc. *1*, e78.

STAR★METHODS

KEY RESOURCES TABLE

REAGENT or RESOURCE	SOURCE	IDENTIFIER
Bacterial and virus strains		
Escherichia coli (*E.coli*; Gram-negative)	ATCC	ATCC 25922
Staphylococcus aureus (*S. aureus*; Gram-positive)	ATCC	ATCC 35556
Chemicals, peptides, and recombinant proteins		
Hyaluronic acid sodium slat-Average MW 1.0-2.0 million Da	BIOSYNTH Carbosynth	CAS No:[9067-32-7]
Gelatin from porcine skin Bloom 175, Type A	Sigma Aldrich	CAS Number:9000-70-8; G2625-500G
Sodium Periodate ($NaIO_4$)	TORONTO RESEARCH CHEMICALS INC.	Cat#S665000
Ethylenediamine (99%)	Sigma Aldrich	CAS Number:107-15-3; E26266-500ML
Ethylene glycol	Sigma Aldrich	CAS Number:107-21-1; 324558-100ML
L-lysine monohydro-chloride	Sigma Aldrich	CAS Number: 657-27-2; L8662-256
1-ethyl-3-(3-dimethylaminopropyl) carbodiimide hydrochloride (EDC)	Thermo Fisher Scientific	CAS Number:25952-53-8; 22981
N-Hydroxyscucinimide (NHS), 98%	Sigma Aldrich	CAS Number:6066-82-6; 130672-100g
25% glutaraldehyde	Sigma Aldrich	CAS Number: 111-30-8; G6257-100ML
Spectra/Por 3 Dialysis membrane MWCO:3.5 kD	Spectrum laboratories, InC.	Cat#08-670-5C
Spectra/Por 4 Dialysis MWCO: 12-14 kD	Spectrum laboratories, InC.	Cat#08-667E
Hyclone phosphate buffer saline (1X).0067M (PBS)	HyClone Laboratories	Cat#SH30256.01
cytiva DMEM/LOW GLUCOSE	HyClone™	Cat#SH30021.01
Difco™ Nurient Agar	Difco Laboratories, Becton, Dickinson and Company	213000
Difco™ Nurient Broth	Difco Laboratories, Becton, Dickinson and Company	234000
Recombinant Human FGF-basic (154 a.a.)	PEPROTECH	Cat#100-18B-100UG
Trizol LS Reagent	Ambion by Life technologies, Thermo Fisher Scientific	Cat#10296010
Power SYBR Green PCR master Mix	Thermo Fisher Scientific	Cat#4367659
TNBS 1% solution in methanol	GBioscience	CAS# 2508-19-2; F.W. 293.17
Sodium bicarbonate (reagent grade)	Sigma Aldrich	CAS Number: 144-55-8; S6014
Sodium dodecyl sulfate	Sigma Aldrich	CAS Number: 151-21-3; 436143-25G
Corning Matrigel Matrix	Life Science	Cat#354277
Hydrochloric acid (HCl) ACS reagent, 37%	Sigma Aldrich	CAS Number: 7647-01-0; 320331-500ML
Streptozocin ≥ 75% α-anomer basis,≥ 98%(HPLC), powder	Sigma Aldrich	CAS Number: 18883-66-4
Glycine	Merck	CAS Number: 56-40-6; 410225
Critical commercial assays		
Live/DeadTM Viability/Cytotoxxicity Kit	Invitrogen by Thermo Fisher Scientific	Cat#L3224
Cell Counting Kit-8 assay (CCK-8)	Dojindo Laboratories, Kumamoto, Japan	CK04
hematoxylin and eosin (H&E)	N/A	N/A

(*Continued on next page*)

Continued

REAGENT or RESOURCE	SOURCE	IDENTIFIER
Masson trichrome staining (MT)	N/A	N/A
TAKARA. PrimeScript™ RT Reagent Kit (perfect real time), 200 Rxns	Takara Bio Inc.	Cat# RR037A
Experimental models: Cell lines		
Human adipose derived stem cells (hASC)	Chung-Ang University	N/A
Raw 264.7	Korean Cell Line Bank	KCLB No. 40071; RRID:CVCL_0493
Streptozoltocin-induce diabetic C57BL/6 mice (C57BL/6NCrl)	Animal Lab	Code 24982426-2575
Oligonucleotides		
GAPDH F: GGT GCT GAG TAT GTC GTG GA R: GTG GTT CAC ACC CAT CAC AA	Bioneer	OLG-211206-130 OLG-211206-130
CD68 F: GCC CGA GTA CAG TCT ACC TGG R: AGA GAT GAA TCG TGC GCC AT	Bioneer	OLG-211230-112 OLG-211230-112
COL1a1 F: TGT TCA GCT TTG TGG ACC TC R: TCA AGC ATA CCT CGG GTT TC	Bioneer	OLG-211206-130 OLG-211206-130
COL3a1 F: CGG TGA ACG GGG CGA AGC TGG TT R: GAC CCC TTT CTC CTG CGG CTC CT	Bioneer	OLG-211206-130 OLG-211206-130
TNF-α F: AGC CCA CGT CGT AGG AAA CCA R: TGT CTT TGA GAT CCA TGC CGT TGG C	Bioneer	OLG-211206-134 OLG-211206-134
TGF-β1 F: CCT GAG TGG CTG TCT TTT GAC R: ACA AGA GCA GTG AGC GCT GAA T	Bioneer	OLG-211230-112 OLG-211230-112
IL-1β F: TTT GAC AGT GAT GAG AAT GAC CTG TTC R: TCA TCA GGA CAG CCC AGG TCA AAG	Bioneer	OLG-211206-134 OLG-211206-134
α-SMA F: TTT GAC AGT GAT GAG AAT GAC CTG TTC R: TCA TCA GGA CAG CCC AGG TCA AAG	Bioneer	OLG-211206-130 OLG-211206-130
VEGFA F: TCG TCA AGT GTA GGT CCC ATA R: CCT TCC ACA ATG CCA AAG TT	Bioneer	N/A
Software and algorithms		
Image J software	ImageJ	https://www.imagej.nih.gov
Prism 6	GraphPad	https://www.graphpad.com/features
Real time PCR system software	StepOnePlus Real-Time PCR system (AB Applied, Life Technologies, MA).	Step One™ Soft ware Version 2.3
ImageFocus 4 English Version	Euromex microscopes Holland	https://www.euromex.com
NIS-Elements	Nikon software	https://www.microscope.healthcare.nikon.com

RESOURCE AVAILABILITY

Lead contact

Further information and requests for resources and reagents should be directed to and will be fulfilled by the lead contact, Professor Hansoo Park (heyshoo.cau.ac.kr).

Materials availability

This study did not generate we unique reagents and hydrogel samples generated in this study are available on a reasonable request from the lead contact, Professor Hansoo Park (heyshoo@cau.ac.kr).

Data and code availability

- Data. All data reported in this paper will be shared by the lead contact upon request.
- Code. This paper does not report original code.
- Any additional information required to reanalyze the data reported in this paper is available from the lead contact upon request.

EXPERIMENTAL MODEL AND STUDY PARTICIPANT DETAILS

Diabetic mice model

The animal experiment protocol was approved by the Institutional Animal Care and Use Committee at Chung-Ang University (approval number: IACUC-CAU-A2022046), and all experiments were performed in the Animal Research Laboratory of Chung-Ang University in compliance with institutional guidelines. In the experiment, we induced type 1 diabetes mellitus in male mice C57BL/6 (Animal Lab, 24982426-2575) using a specific protocol involving the repeated administration of low doses of streptozotocin. We prepared streptozotocin (Sigma Aldrich, 1883-66-4) with sodium citrate buffer at a concentration of 4 mg/mL. Each mouse received intraperitoneal injections for five consecutive days (from day 1 to day 5) at a dose of 40mg/kg, which was adjusted based on the weight of each mouse (1.0 mL/100g). On day 14, we conducted fasting blood glucose level analysis using blood samples obtained from the tail vein of each mouse. If the blood glucose concentration exceeded 150 mg/dL, we considered diabetes to have been induced. If less than 40% of the group did not meet these criteria, we had planned to perform the fasting blood sugar test on day 28. However, we were fortunate to find that all the mice met the diabetes criteria by day 14 in our experiment.[69]

We performed an *in vivo* investigation to assess wound contraction and histological alterations in male C57BL/6 mice aged 6-8 weeks, with each mouse weighing around 20-25 g, see Figure S4. Following the induction of type 1 diabetes in these mice using a protocol involving repeated low doses of streptozotocin, we created four 8 mm wounds on the back of each mouse using a punch biopsy. Wounds were then treated with various dressing hydrogels, including a control group with saline, HGel, HGel-FGF-b, and HGel-GNPs-lysine-FGF-b. Changing hydrogel dressing was performed over a 14 days Wound healing progress was assessed by capturing photographs on days 1, 4, 7, 10, and 14. Histological samples were collected from half of the groups, each consisting of 8 mice, on days 7 and 14.

hASC culture

The use of hASCs was approved by the Chung-Ang University Hospital Institutional Review Board and conducted as specified by the guidelines of the Declaration of Helsinki (IRB No. 2151-005-463). Isolation and characterization methods of hASCs are describe in our previous publication.[70] hASCs were cultivated utilizing Dulbecco's modified Eagle's medium low-glucose (Low-DMEM) (obtained from HyClone Laboratories, Logan, UT), supplemented with 10% fetal bovine serum (FBS) (HyClone) and 1% antibiotic/antimycotic solution (HyClone). The harvested cultured cells were detached using a 0.25% trypsin solution (HyClone) at a concentration of 1×. hASCs were incubated in an incubator (HERAEUS BB 15, Thermo Fisher Scientific, Seoul, Korea) at 37°C with 5% CO_2. The culture media was changed every two days.

Raw 264.7 culture

Raw 264.7 (KCLB No. 40071) received from Korean Cell Line Bank. Raw 264.7 were cultured utilizing Low-DMEM, supplemented with 10% FBS and 1% antibiotic/antimycotic solution. The harvested cultured cells were detached using cell scraper. Raw 264.7 were incubated in an incubator (HERAEUS BB 15, Thermo Fisher Scientific, Seoul, Korea) at 37°C with 5% CO_2. The culture media was changed every two days. Cell lines were tested for mycoplasma contamination.

Microbe strains

Two bacteria species were used in this study. *E.coli* (ATCC 25922) and *S. aureus* (ATCC 35556). Agar plates (Difco Laboratories, 213000) and LB broth (Difco Laboratories, 234000) were made for growing each of these bacterial species. Plate were stacked using the quadrant streaking method. Bacteria species were incubated in an incubator (HERAEUS BB 15, Thermo Fisher Scientific, Seoul, Korea) at 37°C.

METHOD DETAILS

Preparation of gelatin GNPs through a two-step desolvation method

The desolvation technique, as outlined by Coester C. J., was employed for GNPs fabrication.[71] To precipitate high molecular weight gelatin, 2.5 g of gelatin (Sigma Aldrich, 9000-70-8; G2625) was dissolved in 50 mL of distilled water, and then 50 mL of acetone was added. The precipitated gelatin was re-dissolved in 50 mL of distilled water, agitated at 700 rpm at 40°C, and the pH was adjusted to 2.5 using 1 M hydrochloric acid (HCl) (Sigma Aldrich, 7647-01-0; 320331). Formation of GNPs was initiated by the dropwise addition of 150 mL of acetone, followed by a 15 h cross-linking process with 0.25% glutaraldehyde (Sigma Aldrich, 111-30-8; G6257). The reaction was terminated by adding a 0.1 M glycine solution (Merck, 56-40-6; 410225). The GNPs were isolated via centrifugation at 12,000 rpm and then underwent freeze-drying for 48 h.

GNPs-lysine preparation

Native GNPs underwent further conjugation with ethylenediamine and L-lysine (Sigma Aldrich, 657-27-2; L8662-256) at pH 4.5. EDC (Thermo Fisher Scientific, 25952-53-8; 22981)/NHS (Thermo Fisher Scientific, 6066-82-6; 130672) was utilized to activate the lysine carboxylic groups, and the reaction with ethylenediamine was carried out for one h at room temperature. The activated GNPs were then added to the activated lysine solution. The process was allowed to proceed for four h. The GNPs-lysine complex was resuspended three times in distilled water and subsequently subjected to freeze-drying at –80°C. Finally, a fine, light-yellow GNPs-lysine powder was obtained.

Determination of nanoparticle size distribution

The particle size distribution was determined using a dynamic light scattering technique, performed at 25°C with a 35 mW He-Ne laser at a light-scattering angle of 90° in triplicate using a Zetasizer Nano ZS instrument. The scattering intensities were analyzed using software provided by Malvern.

Preparation of oxidized hyaluronic acid (Oxi-HA)

Oxi-HA containing aldehyde groups was prepared by reacting HA (BIOSYNTH Carbosynth, 9067-32-7) with $NaIO_4$.[72] Briefly, 1.0 g of HA was dissolved in 100 mL of distilled water at a concentration of 1.0 %. Then, $NaIO_4$ (TORONTO RESEARCH CHEMICALS INC, S665000) 0.574 g was added to the HA solution. The aqueous reaction solution was then continuously stirred using a magnetic stirrer for 24 h at room temperature. Ethylene glycol (Sigma Aldrich, 107-21-1; 324558) (1.0 mL) was added to inactivate any unreacted $NaIO_4$. The solution was then thoroughly dialyzed (MWCO, 12,000–14,000) (Spectrum laboratories, InC., 08-667E) against distilled water for three days. Finally, the solution was freeze-dried at –80 C for 48 h.

Preparation of amine gelatin (Gel)

Gelatin was dissolved in PBS at a final concentration of 5.0% at 37°C. Ethylenediamine (Sigma Aldrich; 107-15-3; E26266) and EDC were added to the gelatin solution with a molar ratio 1:2:40 [carboxyl groups on gelatin chains: EDC: ethylenediamine]. Immediately after adding the reagents, the pH of the solution was adjusted to 5.0 by adding HCl. The reaction mixture was agitated at 37°C for 18 h and dialyzed (MWCO, 3,500) (Spectrum laboratories, InC., 08-670-5C) (against distilled water for 48 h to remove the excess ethylenediamine and EDC. The dialyzed solution was freeze-dried at –80°C to obtain the modified gelatin.[33]

Characterizations of Oxi-HA, Gel, GNPs, and GNPs-lysine

FTIR spectra were measured to validate the anticipated pendant functionalities. ^{1}H-NMR spectra were conducted at room temperature using a Varian 600 spectrometer, with tetramethylsilane (TMS) as an internal reference. HA, gelatin, Oxi-HA, and Gel were dissolved in D_2O for the ^{1}H-NMR analysis. The quantification of free amine groups in both GNPs and GNPs-lysine was performed using a colorimetric trinitrobenzene sulfonic acid (TNBS) assay (GBioscience. 2508-19-2; F.W. 293.17) GNPs and GNPs-lysine were directly assessed in a reaction buffer, Sodium bicarbonate (Sigma Aldrich,144-55-8; S6014) at concentrations ranging from 20 to 200 μg/mL. The reaction mixture was incubated at 37°C for 2 h. Subsequently, Sodium dodecyl sulfate (SDS) (Sigma Aldrich, 151-21-3; 436143) solution and 1N HCl were added to each sample, and the absorbance of the solutions at 335 nm was measured. A standard curve was generated using cysteine dissolved in various known concentrations to determine the quantity of amines presented in the GNPs and GNPs-lysine.

Hydrogel fabrication and gelation time measurement

In a glass test tube, 300 μL of a 20% Oxi-HA solution was mixed with 700 μL of a 20% Gel solution at 200 rpm using a magnetic bar at 37°C. The time required for the magnetic bar to stop was recorded as the gelation time of the mixed solution.

Swelling and degradation properties

The swelling analysis of the hydrogels was conducted gravimetrically. PBS (HyClone, SH30256.01) was used to maintain the pH at 7.4 and the swelling temperature at 37°C. The hydrogel samples were removed from the buffer solution at certain times and weighed after removing the excess water with filter paper. The equilibrium swelling was calculated using the following equation:

$$Equilibrium\ swelling\ (\%) = \left[\frac{W_s - W_i}{W_i}\right] \times 100$$

In the equation, W_i refers to is the initial hydrogel weight, and W_s refers to the equilibrium weight of the swollen hydrogel.

The *in vitro* degradation of the hydrogels was performed under simulated physiological conditions. Briefly, the dried hydrogel was weighed (*Wi*) and subsequently incubated at 37°C in 1.0 mL of PBS (pH 7.4). At specific time points (1, 3, 7, and 14 days), the samples were carefully withdrawn from the degradation medium, and water on the surface of the hydrogel was removed by filter paper. The degraded

hydrogel samples were freeze-dried, lyophilized for 48 h, and weighed (W_t). The percentage of weight remaining was calculated using the following equation:

$$Percentage\ of\ weight\ remaining\ (\%) = 100 - \left[\frac{W_i - W_t}{W_i}\right] \times 100$$

Morphology

The freeze-dried hydrogel samples were analyzed using a SEM (SEM; S-3400N, Hitachi, Tokyo, Japan). The samples were sectioned using a scalpel to obtain cross-sections, which were then coated by sputtering. The SEM analysis was performed using secondary electron imaging. Different magnifications were used to evaluate the surface morphology of the samples. An accelerating voltage of 5 kV was used during the imaging process.

Rheological properties

A rheometer (Model ARES-G2) instrument with parallel plate geometry was used to evaluate the viscoelastic behavior of the hydrogel by performing oscillation frequency sweep tests. Hydrogels were prepared by mixing the reaction solutions and placed onto the center of the bottom plate of the rheometer. The storage modulus (G′) and loss modulus (G″) were measured as a function of angular frequency using the parallel plate geometry over a frequency range of 1–10 rad/s at a constant amplitude ($\gamma = 1\%$).

Measurement of adhesion ability

To assess the adhesive properties of the hydrogels, the experiment utilized porcine skin as a substitute for human skin. Briefly, Oxi-HA and Gel were dissolved in PBS, and these solutions were applied to the surfaces of two pieces of porcine skin. Each piece of porcine skin was coated with hydrogel solution, covering an area of approximately 2x2 cm^2. Subsequently, the treated skin samples were put together, and the adhesive strength of the hydrogels was evaluated using a universal testing machine (UTM; Model: TCK-K010).

Biocompatibility and cell migration

The Live/Dead kit (0.1 mM calcein AM, 0.4 mM ethidium bromide homodimer-1; Invitrogen, L3224) was employed to assess biocompatibility in a humidified cell incubator with 5% CO_2 at 37°C. A suspended solution of hASCs (p = 5; cell concentration: 0.5 x 10^6) was seeded onto a 24-well plate and incubated for 24 h. GNPs and GNPs-lysine, ranging from 10-30 mg, were suspended in culture media, and 10.0 μL of each nanoparticle was added to individual wells of the hASCs culture plate. The nanoparticles treated with hASCs were subsequently washed with PBS and stained with the Live/Dead kit at specified time intervals. After 30 min, the samples were observed using a fluorescence microscope (Model: CCD5; DC12V/2A; Euromex microscopes).

The impact of GNPs and GNPs on cell proliferation was subsequently assessed. Following the manufacturer guidelines, cell proliferation was measured on days 1, 3, and 7 using CCK-8 assay (CCK-8; Dojindo Laboratories, Kumamoto, Japan, CK04). In brief, hASCs treated with nanoparticles were rinsed with PBS and then immersed in a mixed solution of 10% CCK-8 reagent with fresh medium at 37°C for 2 h. The absorbance at 450 nm was recorded using a plate reader (Synergy H1 Hybrid Reader; BioTek).

To assess the hydrogel efficacy in promoting cell proliferation and to determine whether it established a conducive microenvironment for cell culture. Initially, 10 μL of each hydrogel was applied to a 24-well plate for 15 min, followed by rinsing with PBS. Subsequently, hASCs (p = 5; cell concentration: 1 × 10^6 cells/mL) were then seeded onto HGel, HGel-GNPs, and HGel-GNPs-lysine, with 500 mL of culture media added to each well. As a positive control, hASCs treated with Matrigel (Life Science, 354227) were prepared using the same method as for HGel. The evaluation of cell proliferation was measured on days 1, 3, and 7 using the CCK-8 assay, following the same procedure as for hASCs treated with nanoparticles.

The impact of FGF-b (PEPROTECH, 100-18B) on promoting hASC proliferation was investigated through CCK-8 analysis at concentrations of 0.1 μg/mL, 1.0 μg/mL, and 10.0 μg/mL. Additionally, FGF-b was assessed for its influence on the migration of macrophages (Raw 264.7; KCLB No. 40071). Macrophages were cultured in low-DMEM supplemented with 10% FBS and 1% antibiotic/antimycotic solution. A linear scratch was created using a sterile pipette tip to induce wounds, and the cells were subsequently treated with FGF-b at concentrations of 0.1 μg/mL, 1.0 μg/mL, and 10.0 μg/mL. The progression of wound healing was photographed at 0h, 2h, 6h, 12h, and 24 h under an optical microscope (Model: Nikon ECLIPSE TS100, NIS-Elements3m).

Antibacterial ability test

To examine the antibacterial properties of the hydrogels, Gram-negative *E. coli* and Gram-positive *S. aureus* were employed. DifcoTM Nutrient Agar (213000) and DifcoTM Nutrient Broth (234000) served as the culture media. The antibacterial activities of the hydrogel were assessed through ZOI testing and OD measurements. For the ZOI experiment, *E. coli* and *S. aureus* were inoculated onto plates. Hydrogels, including HGel, HGel-GNPs, and HGel-GNPs-lysine, were placed on the plates, and the incubation occurred at 37°C for 12 h. Regarding the OD test, the prepared hydrogels were introduced into a bacterial medium (1×10^6 CFU/mL for *S. aureus* and 1.4×10^6 CFU/mL for *E. coli*), incubating for 2, 4, 6, 8, 12, and 24 h.

The bacterial cultures treated with normal saline and 75% ethanol were used as positive and negative controls, respectively. The OD change was measured at 600 nm using a spectrophotometer. The tests were performed in triplicate. In addition to the *in vitro* antibacterial

activity, the morphology of the bacteria was observed by SEM to assess the antibacterial properties of the composite hydrogel. The bacterial cultures were fixed with 2.5% glutaraldehyde and gradually dehydrated using ethanol. Finally, the samples were lyophilized and sputter-coated before observing the bacteria morphology.

In vivo wound healing assay

The wound healing efficacy of hydrogels was evaluated using a diabetic mice model (C57BL). Diabetes was induced in C57BL mice using the low-dose STZ injection method.[73] After removing dorsal hair, four full-thickness circular wounds, each measuring 8 mm in diameter, were created on the back using a needle biopsy. Silicone sheets were then applied around the wounds. Subsequently, each wound received one of the following treatments: saline as a control, FGF-b, HGel + FGF-b, and HGel-GNPs-lysine + FGF-b. The wound size was assessed using Image J software, and the percentage of wound area at days 1, 4, 7, 10, and 14 was calculated using the provided equation:

$$\textit{Percentage of wound area}\ (\%) = \left[\frac{A_i}{A_o}\right] \times 100$$

In the equation, A_o refers to the original (day 1) area of the wound site, and A_i refers to the area for the wound site at the time of measurement.

Histology evaluation

For histological examination, the skin tissues from the wounds were isolated and promptly fixed in 4% formaldehyde. Subsequently, the tissues were embedded in paraffin and cut into 4-μm-thick slices for H&E staining. For epidermis thickness, granulation tissue thickness, and collagen densities, we used H&E-stained slides and MT-stained slides to obtain optical microscopy tissue images. Quantitative data was analyzed using Image J software. A minimum of three random areas per groups were chosen for analysis.

Reverse transcription followed by quantitative polymerase chain reaction

Total RNA was extracted from biopsy tissue using Trizol LS reagent (Thermo Fisher Scientific, 10296010) according to the manufacturer's instructions. Then, 1.0 μg of RNA was used to synthesize cDNA by reverse transcription (RT) using the TAKARA. PrimeScript™ RT Reagent Kit (Takara Bio Inc. RR037A). The synthesized cDNA was stored at −20 °C until use. Quantitative polymerase chain reaction (qPCR) analysis was performed using the Power SYBR Green PCR Master Mix (Thermo Fisher Scientific, 4367659) on a StepOnePlus Real-Time PCR system (AB Applied, Life Technologies, MA). The primer sequences for the glyceraldehyde 3-phosphate dehydrogenase (GAPDH) reference gene and the target genes were shown in key resources table. The expression level of each target mRNA was normalized to that of GAPDH and compared with that of the control group.

QUANTIFICATION AND STATISTICAL ANALYSIS

Randomization was used to assign the various samples to the experimental groups and treatment conditions for all *in vitro* and *in vivo* studies. The statistical parameters and the number of samples per experiment are found in the figure ligands. Cell culture experiments were collected from three or four independent cultures for each treatment group. Representative of H&E staining and MT staining images were obtained from at least three to five replicates per group. Image J software was used to quantified remaining scratch wound area percentage, epidermis thickness, granulation tissue thickness, and collagen densities. The data was analyzed using one-or two-way ANOVA followed by Tukey's test for multiple comparisons on GraphPad Prism 8.0. A value of $P < 0.05$ was considered to be statistically significant in all the experiments. All quantitative results were represented as mean ± SD. Excel was used for raw data collection, analysis, and quantification. Illustrations and experiments designs were created using Power Point and Biorender (https://www.biorender.com/).